culture medium under a humidified atmosphere. To establish MEFs expressing exogenous *mDomino*, the *mDom*$^{fl/fl}$*;CreER* MEFs were transfected with the pNEF-DomHA plasmid encoding a neomycin-resistance gene and the C-terminally HA-tagged mDomino cDNA (1/2-disrupted Myc-mDomino-HA (4)) by electroporation using the Amaxa system (Amaxa), and stable transfectants were selected by G418 resistance.

Cell-cycle Analysis—Cells were trypsinized and fixed in 70% ethanol overnight at −20 °C, treated with 100 μg/ml RNase A (Sigma) in phosphate-buffered saline (PBS) for 30 min at room temperature, and then incubated with 40 μg/ml propidium iodide in PBS for 30 min on ice. Data were acquired using a FACSCalibur (BD Biosciences) and analyzed using Flow-Jo software (TreeStar, Inc.).

Microarray Analysis—For DNA microarray analysis, RNA was extracted from *Dom*$^{fl/fl}$*;CreER* MEFs that were left untreated or treated with 7.5 nM OHT for 8 h and then cultured for 2 days. Biotin labeling of complementary RNA was performed using the GeneChip 3′ IVT Express kit (Affymetrix). The biotinylated RNA was fragmented and hybridized to Mouse Gene 430 2.0 chips (Affymetrix) as per the manufacturer's protocol. Both raw image (.dat) and intensity (.cel) files were generated using Gene Chip Operating Software (Affymetrix). All the data, including the signal intensity of each gene, were determined with Microarray Analysis Suite Version 5.0 (Affymetrix). The overall signal intensity of each array was normalized so that the average would be 500. The -fold change analysis was done using the average of OHT-untreated MEFs ($n = 3$) relative to the average of OHT-treated MEFs ($n = 3$). p values were calculated using Student's t test. The data were filtered for a change in expression exceeding 2.0-fold and a p value of <0.015. In addition, in the assessment of down-regulated genes, genes presenting with a negative value in at least one of the three profiles or with an average intensity of <100 were deleted in the profiles of OHT-untreated MEFs.

Real-time PCR for the Quantitative Analysis of mRNA—For the reverse-transcribed (RT)-PCR reaction, cDNA was synthesized from DNase I-treated total RNA (0.5 μg) using an oligo(dT) primer and Superscript III (Invitrogen) in a 10-μl reaction mixture. Quantitative real-time RT-PCR was carried out using the LightCycler 480 SYBR Green system (Roche Diagnostics), as described before (31), under the following conditions: 10 s at 95 °C, 10 s at 60 °C, and 20 s at 72 °C for 40 cycles. The primer sets used were: 5′-AGCGTTAAGCAGGAACTGGA-3′ and 5′-TCTGCTGTGATTCCAAGTGC-3′ for FoxM1, 5′-TCACTTCTGGCTACATCCCC-3′ and 5′-ATAGGACTCCGTGCCATCAC-3′ for PLK1, 5′-TGAGGAGAAGCAGTGAGGAA-3′ and 5′-CTGAGAGGTATTCTTAGCCT-3′ for CENP-F, 5′-GGGAGAACTTTCCAGGTGTC-3′ and 5′-AGAGAGACTCATCGAGCGAG-3′ for Skp2, 5′-GTGGGTCAGCGCCACACCTC-3′ and 5′-GGGAGAGGCGCTTGTGCAGG-3′ for p53, 5′-TGGCTGGCGGTAAGGCTGGA-3′ and 5′-ACGTCCGTGGCTGGTTGTCC-3′ for H2A.Z, 5′-GGACTGTATGTGGAGCGGTT-3′ and 5′-GAATCGGACGAGGTACAGGA-3′ for c-Myc, and 5′-CCCAGCGCCTGGCCTATGTG-3′ and 5′-TGCAGTCCGGTCCTCCCCAG-3′ for E2F1. All the PCR data were normalized to standards and expressed as copy numbers of target mRNA per nanogram of total RNA.

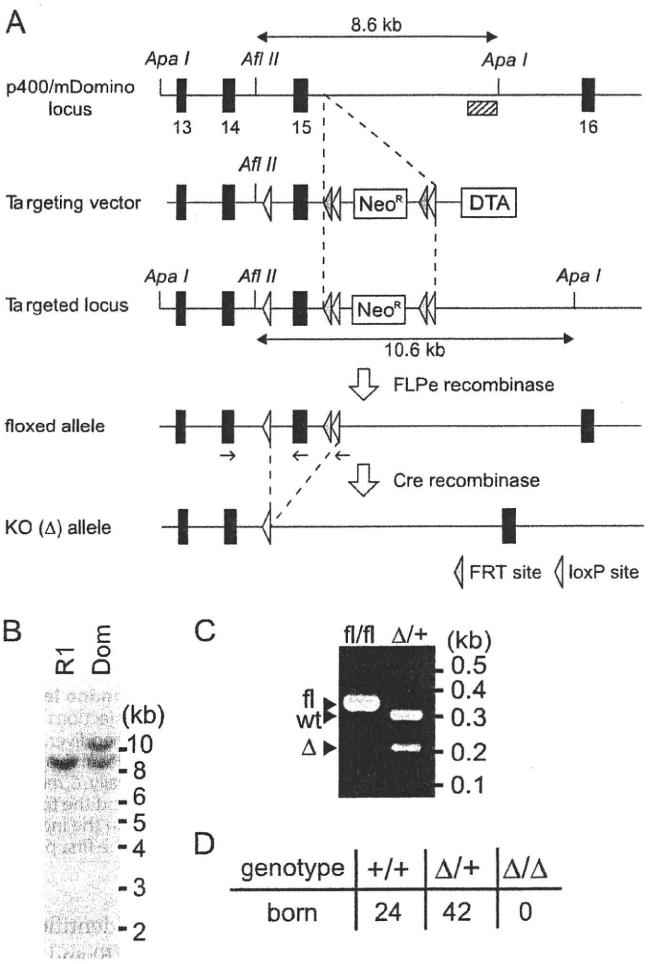

FIGURE 1. **p400/mDomino is essential for embryonic development.** *A*, schematic illustration of the exon organization of the p400/mDomino gene and targeting strategy. A targeting vector was designed in which exon 15 was flanked by two loxP sites, and an *FRT/loxP*-flanked Neo cassette (*NeoFRT*) was inserted into intron 15. Removal of the *NeoFRT* cassette by FLPe recombinase generated the *mDom*^{fl} allele. Cre-mediated recombination between the loxP sites generated the exon-15-deleted allele (*mDom*$^{\Delta}$). The positions of the primers used for genotyping are indicated by *short arrows*. *B*, Southern blot analysis of a correctly targeted ES clone. Genomic DNA from parental (*R1*) or targeted (*Dom*) ES cells was digested with ApaI and AflII, and analyzed by Southern blotting using the probe indicated by the *hatched box* in *A*. The WT and targeted mDom alleles were predicted to result in 8.6- and 10.6-kb bands, respectively, as shown in *A*. *C*, PCR genotyping of *mDom*$^{fl/fl}$ and *mDom*$^{\Delta/+}$ mice. *D*, genotype analysis of the progeny from *mDom*$^{\Delta/+}$ heterozygous matings.

RESULTS

Generation of p400/mDomino Conditional Knock-out Mice—The targeting construct that was designed to delete exon 15 of the *mDomino* gene by Cre-mediated recombination is shown in Fig. 1*A*. The deletion of exon 15 from the *mDomino* locus is expected to remove the catalytic center of the ATPase domain and to generate a mutant mDomino that lacks a major portion (encoded by exons 15–52) of the protein (4). We used an *FRT*- and *loxP*-flanked Neo cassette (*NeoFRT*) and a DTA cassette as positive and negative selection markers, respectively, for homologous recombination. Mouse ES cell clones containing

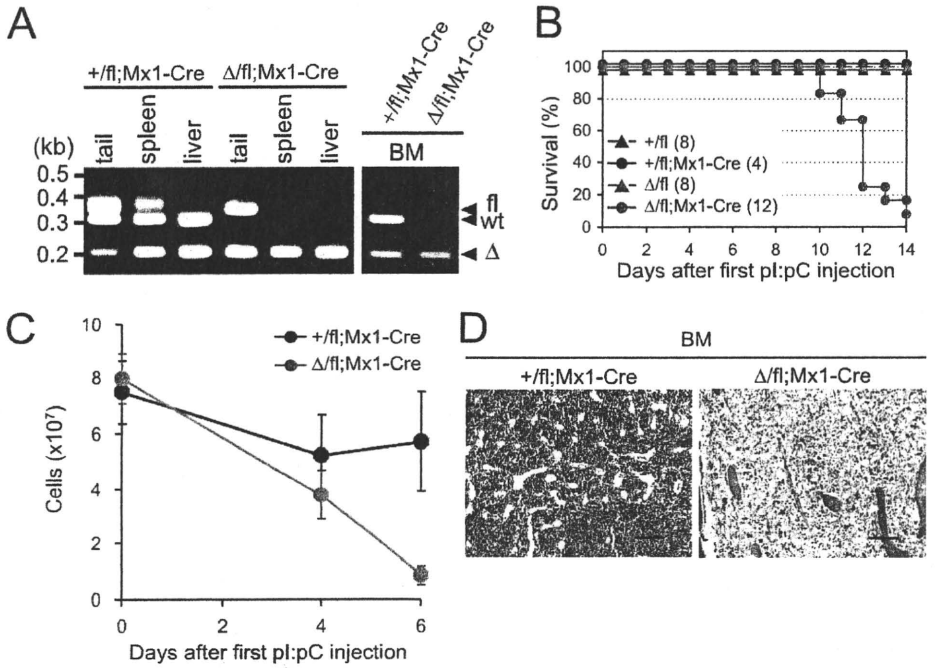

FIGURE 2. **Mx1-Cre-mediated conditional deletion of mDomino leads to rapid mortality and a loss of bone marrow cells.** Mice were given three intraperitoneal injections of pI:pC, one each on days 0, 2, and 4, and then analyzed. *A*, PCR genotyping of DNA from the tail, spleen, liver, and BM was performed on day 6 for the pI:pC-treated $mDom^{+/fl}$;*Mx1-Cre* and $mDom^{\Delta/fl}$;*Mx1-Cre* mice. *B*, survival of the pI:pC-treated $mDom^{\Delta/fl}$;*Mx1-Cre* mice ($n = 12$) and control mice ($n = 20$ in total) was observed daily. *C*, $mDom^{+/fl}$;*Mx1-Cre* mice (*black*, $n = 3$) and $mDom^{\Delta/fl}$;*Mx1-Cre* mice (*red*, $n = 3$) were treated with pI:pC, and the total number of nucleated BM cells in all the femurs and tibiae from a single mouse was determined on the indicated days. *D*, hematoxylin and eosin staining of a paraffin-fixed section of the femur 8 days after the first pI:pC injection. *Scale bars* represent 100 μm.

the *mDomino*-targeted allele ($mDom^{NeoFRT}$) were identified by PCR (not shown) and Southern blot analyses (Fig. 1*B*) and were used to generate mice carrying the $mDom^{NeoFRT}$ allele in the germ line. Then, the $mDom^{NeoFRT}$ mice were crossed with *CAG-FLPe* transgenic mice (25) to remove the *NeoFRT* cassette. The resulting *mDomino* allele containing two *loxP* sites in introns 14 and 15 (the "floxed" allele) was designated as $mDom^{fl}$ (Fig. 1, *A* and *C*). $mDom^{fl/fl}$ mice were obtained from heterozygous matings at a Mendelian ratio and were phenotypically indistinguishable from their wild-type (WT) or heterozygous littermates, indicating that the $mDom^{fl}$ allele was functional (data not shown). We also crossed $mDom^{NeoFRT}$ mice with *E2a-Cre* transgenic mice (26), to obtain an *mDomino* allele lacking exon 15 in the germ line, which was designated as $mDom^{\Delta}$ (Fig. 1, *A* and *C*). Heterozygous $mDom^{\Delta/+}$ mice were born and developed normally, but no homozygous mutant offspring were born from the intercross of $mDom^{\Delta/+}$ mice, indicating that the homozygous $mDom^{\Delta/\Delta}$ mutation is lethal during embryonic development (Fig. 1*D*). We have not determined whether $mDom^{\Delta/\Delta}$ embryos die in a very early stage of embryogenesis, or can develop at least to embryonic day 8.5 as observed in the homozygous embryos expressing the N-terminally deleted mDomino mutant (24).

Acute Loss of Bone Marrow Hematopoietic Cells Caused by the Induced Deletion of mDomino—To generate mice in which the *mDomino* gene was inducibly inactivated, $mDom^{fl}$ mice were crossed with *Mx1-Cre* transgenic mice (*Mx1-Cre*), which carry the Cre gene under the control of the Mx1 promoter. The *Mx1-Cre* gene is induced in adult mice by the administration of poly(I):poly(C) (pI:pC) via interferon (IFN) induction (27). To estimate the efficiency of the *mDom* deletion in adult tissues, pI:pC was administered intraperitoneally to *mDom-floxed* mice three times, once each on days 0, 2, and 4. Two days after the last pI:pC injection, genomic DNA from the tail, spleen, liver, and bone marrow (BM) was analyzed by PCR. Although the deletion of the floxed exon 15 of the $mDom^{fl}$ allele was inefficient in the tail, an efficient deletion of the floxed allele (50–70%) was observed in the spleen, and almost complete deletion was achieved in the liver and BM in the $mDom^{\Delta/fl}$;*Mx1-Cre* and the $mDom^{+/fl}$;*Mx1-Cre* mice (Fig. 2*A*).

To explore the role of mDomino in adult mice, $mDom^{\Delta/fl}$;*Mx1-Cre* mice were injected with pI:pC, as described above. This treatment resulted in the death of almost all of the $mDom^{\Delta/fl}$;*Mx1-Cre* mice within 14 days after the first pI:pC injection, whereas no mortality was observed in any of the pI:pC-injected control mice ($mDom^{+/fl}$; Mx1-Cre, $mDom^{\Delta/fl}$, and $mDom^{+/fl}$) (Fig. 2*B*). Our previous study showed that mice with the N-terminally deleted mDom mutation die during embryonic development with defects in primitive hematopoiesis (24). Therefore, to investigate the roles of mDomino in adult hematopoiesis, we examined the BM phenotypes of the pI:pC-injected $mDom^{\Delta/fl}$;*Mx1-Cre* mice on days 4 and 6 (*i.e.* 0 and 2 days after the last pI:pC injection, respectively), and found a drastic reduction of nucleated cells (Fig. 2*C*). Hematoxylin-eosin staining revealed the obvious disappearance of BM hematopoietic cells, except for the anucleate mature erythrocytes (Fig. 2*D*). These results indicated that the proliferation and maintenance of hematopoietic cells in the BM are severely impaired by the inactivation of mDomino.

To determine which of the BM hematopoietic lineages was affected by the mDomino deficiency, we analyzed the BM cells of pI:pC-treated $mDom^{\Delta/fl}$ mice by flow cytometry. The treatment of control mice, such as $mDom^{+/fl}$;*Mx1-Cre* mice (Fig. 3, *A* and *B*) and $mDom^{\Delta/fl}$ mice (free of *Mx1-Cre*, data not shown), with pI:pC resulted in a significant reduction of bone marrow $B220^+$ B cells and $Ter119^+$ erythroid cells but not of $Mac\text{-}1^+$ or $Gr\text{-}1^+$ myeloid cells, indicating that IFN (and/or pI:pC itself) has some deleterious effect on the lymphoid and erythroid lineages but not on the myeloid lineage. In contrast, the deletion of mDomino in BM cells resulted in a significant reduction of the $Mac\text{-}1^+Gr\text{-}1^{mid\text{-}lo}$ monocyte/macrophage lineage and $Mac\text{-}1^+Gr\text{-}1^{hi}$ granulocyte lineage (Fig. 3, *A* and *B*). The $CD71^+Ter119^{mid\text{-}hi}$ erythroid progenitors were also dimin-

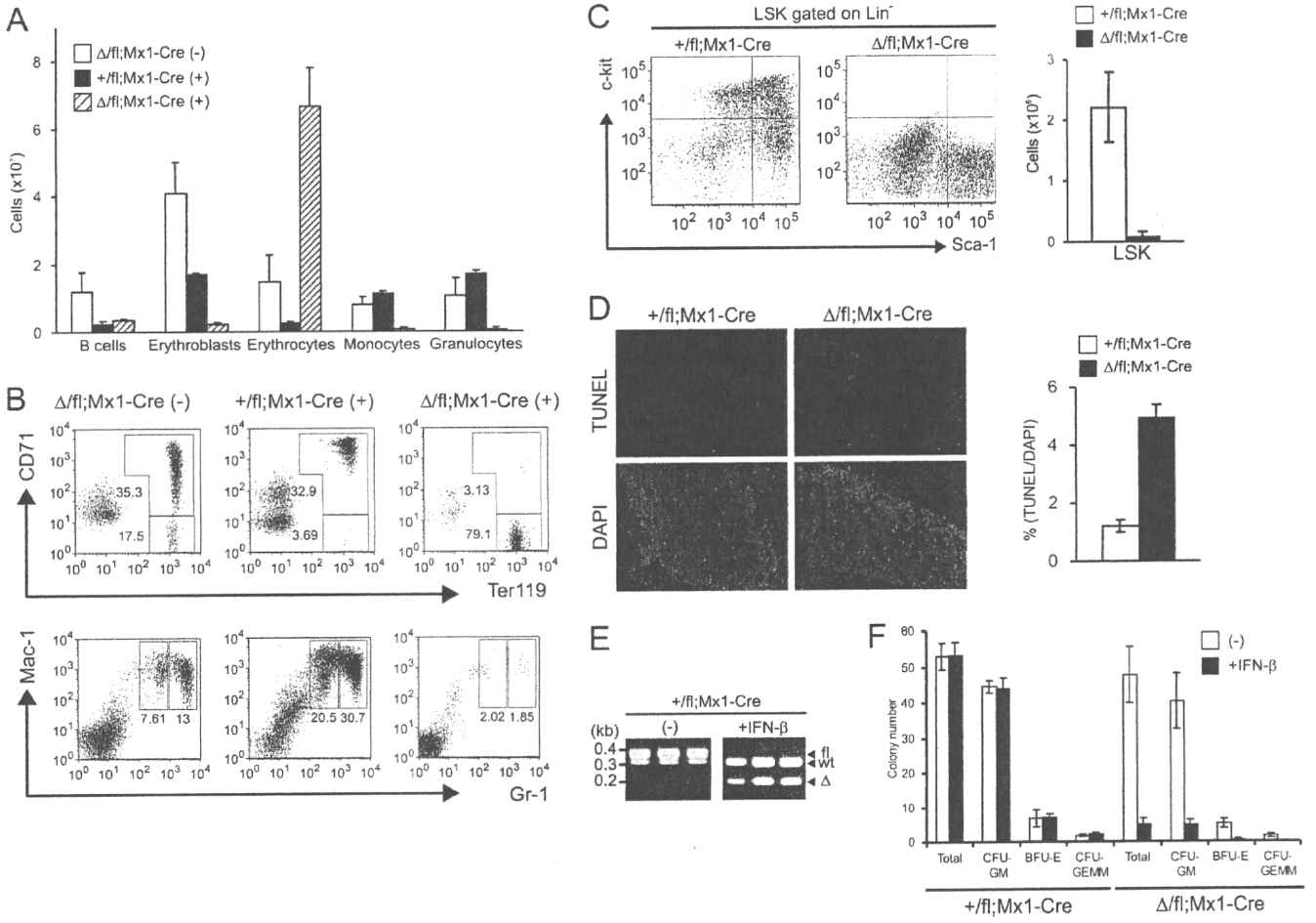

FIGURE 3. **Loss of BM hematopoietic cells by mDomino deletion.** *A*, total number of BM hematopoietic subsets ($n = 3$, mean ± S.E.) in pI:pC-treated (+) or untreated (−) mice on day 4. The number of cells in each subset was calculated from the total number of nucleated BM cells and the flow cytometric analysis of hematopoietic subsets shown in *B*. The hematopoietic subsets were defined by lineage markers as follows: B cells ($B220^+$), erythroblasts ($CD71^{hi}Ter119^{mid}$ and $CD71^{lo\text{-}hi}Ter119^{hi}$), erythrocytes ($CD71^-Ter119^{hi}$), monocytes ($Mac\text{-}1^+Gr\text{-}1^{mid}$), and granulocytes ($Mac\text{-}1^+Gr\text{-}1^{hi}$). *B*, flow cytometric profiles of BM cells from pI:pC-treated (+) or untreated (−) mice on day 4. *C*, flow cytometric analysis of lineage-marker-negative (Lin^-) hematopoietic stem and progenitor cells (*left*), and the total number of $Lin^-Sca\text{-}1^+c\text{-}Kit^+$ (LSK) stem cells (*right*) among the BM cells from pI:pC-injected mice. *D*, apoptotic cell death in the mDomino-deleted BM cells. Cryosections of BM were prepared from pI:pC-injected mice on day 3. The BM samples were stained with TUNEL and counterstained with DAPI (*left*). The TUNEL-positive cells were counted, and the percentage of DAPI-positive cells that were TUNEL-positive was calculated (*right*). *E* and *F*, *in vitro* hematopoietic colony assay of $mDom^{\Delta/fl}$;*Mx1-Cre* BM cells under the induced deletion of mDomino by IFN-β. BM cells (2×10^4 nucleated cells) from $mDom^{+/fl}$;*Mx1-Cre* or $mDom^{\Delta/fl}$;*Mx1-Cre* mice were cultured using the MethoCult M3434 system (Stem Cell Technologies) in 35-mm culture dishes in the presence or absence of 100 units/ml mouse IFN-β (Merck), in duplicate. *E*, three colonies from each of the IFN-treated or untreated (−) cultures of $mDom^{+/fl}$;*Mx1-Cre* BM cells were analyzed for mDomino deletion by PCR. *F*, BM cells were cultured in the presence (*filled bars*) or absence (*open bars*) of IFN-β, and colonies of the colony-forming unit (CFU)-GEMM (granulocyte/erythrocyte/macrophage/megakaryocyte) and CFU-GM (granulocyte/macrophage), and the burst-forming unit of erythroid (BFU-E) containing more than 30 cells were counted after 12 days of culture.

ished when compared with the pI:pC-injected control mice. The reduction in nucleated hematopoietic cells was accompanied by a dramatic increase in $CD71^-Ter119^{high}$ mature erythrocytes, which comprised nearly 80% of the non-adherent cells in the BM cavity (Fig. 3, *A* and *B*). Furthermore, lineage-marker-negative (Lin^-)$c\text{-}kit^+Sca\text{-}1^+$ hematopoietic stem cells and $Lin^-c\text{-}kit^+Sca\text{-}1^-$ progenitor cells were lost in the pI:pC-treated $mDom^{\Delta/fl}$;Mx1-Cre mice (Fig. 3C), indicating that mDomino is necessary for the proliferation and/or maintenance of hematopoietic progenitor/stem cells as well as of committed myeloid cells. To address whether the mDomino-deleted hematopoietic cells underwent apoptosis, we analyzed BM cells using the TUNEL assay. One day after the second pI:pC injection, the BM cells from $mDom^{\Delta/fl}$;*Mx1-Cre* mice displayed more TUNEL-positive cells than the control (Fig. 3*D*). Similar results were obtained by immunohistochemical staining for active caspase-3 (data not shown), indicating that the rapid extinction of nucleated hematopoietic cells from the mDom-deleted BM is, at least in part, due to an increase in their apoptotic cell death.

Next, we examined the effect of mDomino deletion on the *in vitro* growth and differentiation of erythroid and myeloid progenitors using a multilineage colony assay. The BM cells from $mDom^{\Delta/fl}$;*Mx1-Cre* mice or control $mDom^{+/fl}$;Mx1-Cre mice were cultured in methylcellulose medium containing multiple cytokines in the presence or absence of IFN-β. The presence of 100 units/ml IFN-β, which effectively deleted the $mDom^{fl}$ allele (Fig. 3*E*), did not have any deleterious effect on the hematopoietic colony formation (CFU-GM, BFU-E, and CFU-GEMM) of control BM cells (Fig. 3*F*, *left*), but resulted in a drastic reduc-

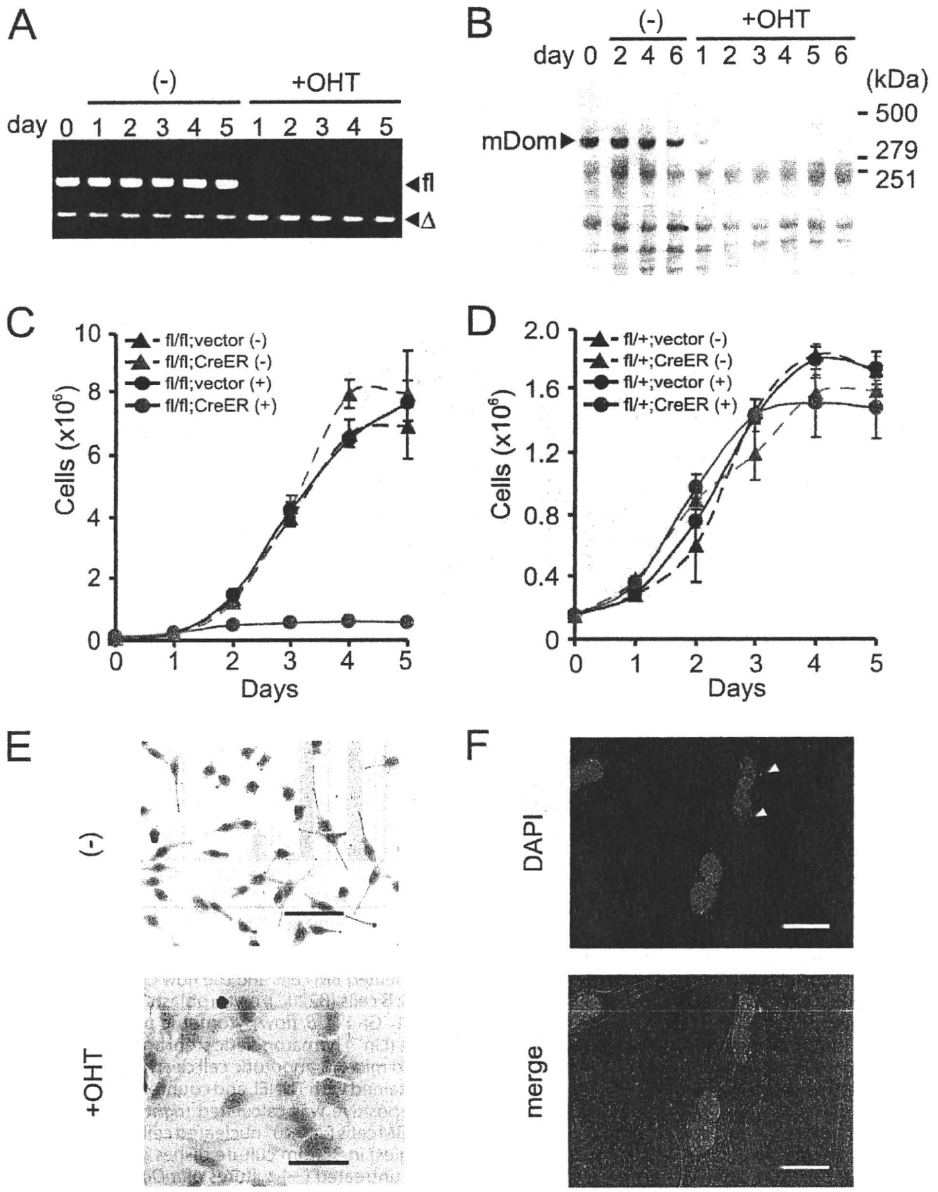

FIGURE 4. **Strong growth inhibition of conditional mDomino-deficient embryonic fibroblasts.** *A*, PCR analysis of the *mDom*^{fl} deletion by OHT. *mDom*$^{fl/fl}$*;CreER* MEFs were left untreated (−) or treated with 7.5 nM OHT for 8 h, washed and further cultured, and then analyzed for the status of the *mDom*^{fl} allele on the indicated days. *B*, Western blot analysis of the mDomino protein in the whole cell lysate of *mDom*$^{fl/fl}$*;CreER* MEFs treated with OHT. *C* and *D*, growth defect of mDomino-deficient MEFs. Four types of retrovirally transduced MEF lines, *mDom*$^{fl/fl}$*;CreER* (*left*), *mDom*$^{fl/+}$*;CreER* (*right*), and their respective vector controls, were left untreated (−) or treated with OHT (+), and then cultured in the normal medium. At the indicated times, the cells were trypsinized and counted. Data are the means ± S.D. of three separate experiments. *E* and *F*, nuclear abnormalities observed in mDomino-deficient MEFs. *E*, Wright-Giemsa staining of the OHT-treated or untreated (−) *mDom*$^{fl/fl}$*;CreER* MEFs after 6 days of culture. *Scale bars* represent 100 μm. *F*, DAPI staining of OHT-treated *mDom*$^{fl/fl}$*;CreER* MEFs (*upper*). *Arrowhead* indicates cells with micronuclei. The DAPI image is *merged* with its bright-field image (*lower*). *Scale bars* represent 25 μm.

tion in the colony formation of the *mDom*$^{\Delta/fl}$*;Mx1-Cre* cells (Fig. 3*F*, *right*). PCR genotyping of the colonies that survived in the IFN-treated *mDom*$^{\Delta/fl}$*;Mx1-Cre* BM culture revealed that the small number of surviving colonies arose from cells that escaped the induced deletion of the floxed mDom gene (data not shown). These results indicated that mDomino-deleted hematopoietic progenitors rapidly, and cell autonomously, lose the ability to proliferate.

mDomino Is Necessary for the Cell-cycle Progression of Embryonic Fibroblasts—The rapid proliferation arrest and/or apoptosis in mDom-deleted BM hematopoietic cells suggested that mDomino could be involved generally in the cell growth regulation. To examine this possibility, we prepared MEFs from *mDom*$^{fl/fl}$ mice and control *mDom*$^{fl/+}$ mice, and immortalized them by the 3T3 passage method. To inducibly inactivate the *mDom*^{fl} allele, the immortalized MEFs were infected with a recombinant retrovirus expressing Cre-ER^{T2} (hereafter simply CreER), which can be activated by treatment with OHT (32). In the CreER-expressing MEFs, the *mDom*^{fl} allele was deleted within a day after OHT treatment (Fig. 4*A*), and the mDomino protein disappeared concomitantly from the cell lysates (Fig. 4*B*). The OHT-induced deletion of mDomino resulted in the rapid and strong growth inhibition of *mDom*$^{fl/fl}$*; CreER* MEFs but not of the vector control *mDom*$^{fl/fl}$ MEFs (Fig. 4*C*). Another control cell line, *mDom*$^{+/fl}$*;CreER* MEF, which was established by the CreER-retrovirus infection of heterozygous *mDom*$^{fl/+}$ MEFs, grew normally even after the induced activation of CreER (Fig. 4*D*). These results indicated that the growth of MEFs is not affected by the addition of OHT or by the activation of the CreER protein and that mDomino is essential for their proliferation. In addition, microscopic examination revealed the emergence of a bi- or multi-nucleated population among the mDomino-deleted MEFs that had an enlarged cell body, abnormal nuclear morphology, and micronuclei (Fig. 4, *E* and *F*).

The above results suggested that mDomino plays an important role in cell-cycle regulation. We therefore analyzed the cell-cycle profiles of mDomino-deleted MEFs by flow cytometry. As shown in Fig. 5 (*A* and *B*), the *mDom*$^{fl/fl}$*;CreER* MEFs treated with OHT showed a significant increase in the population with 4N DNA content and the emergence of polyploid (>4N) cells. To examine the effect of the mDomino deficiency on cell-cycle progression, *mDom*$^{fl/fl}$*;CreER* MEFs were treated with OHT, driven into quiescence by serum starvation, and then released

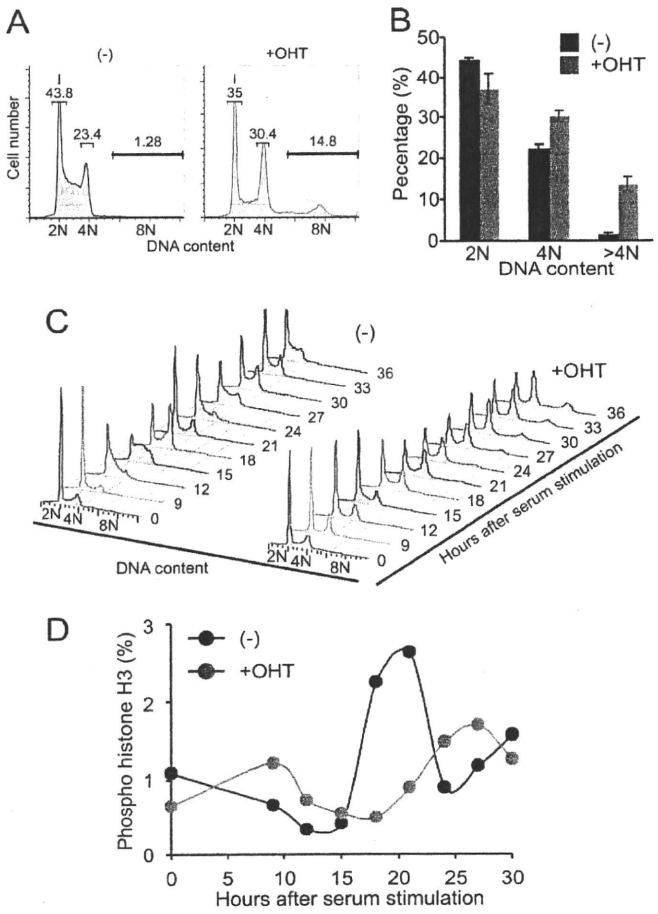

FIGURE 5. **mDomino-deficient MEFs exhibit polyploidy and defective cell-cycle progression.** *A*, the DNA content of OHT-treated or untreated (−) *mDom*$^{fl/fl}$*;CreER* MEFs was determined by flow cytometry after propidium iodide staining. *B*, the percentage of cells with 2N, 4N, and >4N DNA content in *A* was determined in three independent experiments. *C* and *D*, cell-cycle profile of *mDom*$^{fl/fl}$*;CreER* MEFs. Cells were treated with (+) or without (−) OHT for 8 h, serum-starved for 24 h, and then released from the starvation by stimulation with 10% fetal bovine serum. The cells were then collected at the indicated times and subjected to the flow cytometric analysis of their DNA content by propidium iodide staining (*C*), or of the mitotic index by staining with a phospho-Ser-10-specific, anti-histone H3 antibody (*D*).

back into the cell-cycle by the addition of serum. As shown in Fig. 5*C*, the mock-treated cells synchronously entered the S phase 12–15 h after serum stimulation, reached the G_2/M phase at about 18 h, and returned to the G_1 phase at 21 h. In contrast, MEFs treated with OHT displayed a small delay in entering the S phase and a slow but continuous increase in a population with 4N DNA content. This 4N population seemed to include not only the G_2/M population but also an aberrant cell population that had initiated a new round of DNA synthesis without cytokinesis (endoreduplication), which resulted in the accumulation of tetraploid cells with ~8N DNA content. To examine whether mDomino-deficient MEFs entered mitosis, MEFs re-stimulated with serum were stained with a phospho-Ser10-specific anti-histone H3 antibody, and quantified by flow cytometry (Fig. 5*D*). Mock-treated MEFs showed a sharp M-phase peak 18–20 h after stimulation, whereas the mDomino-deficient MEFs showed a delayed entry into mitosis. These results indicated that the depletion of mDomino causes the malfunction of the cell-cycle regulation at multiple steps, especially in the G_2/M phase, and eventually leads to the aberrant mitosis known as "mitotic catastrophe."

p400/mDomino was shown to participate in the adenovirus-E1A-induced transformation process through interaction with the N-terminal region of E1A (3). To examine whether expression of E1A affects the cell cycle defect caused by mDomino deletion, *mDom*$^{fl/fl}$*;CreER* MEFs were infected with retroviral constructs expressing wild-type 12 S E1A or *dl*1102(Δ26–35) mutant that was defective in interaction with mDomino. Resulting MEFs that overexpressed E1A or *dl*1102 grew faster than the parental MEFs or vector control cells, but were growth-arrested soon after the OHT treatment (supplemental Fig. 1), suggesting that overexpression of E1A protein cannot compensate for the mDomino deletion.

To confirm that the observed phenotypes of mDomino-deleted MEFs were caused by the absence of mDomino protein and not by other unexpected events, such as genomic recombination caused by CreER, *mDom*$^{fl/fl}$*;CreER* MEFs were transfected with an expression plasmid for HA-tagged mDomino (pNEF-DomHA), and stable cell lines were analyzed. As shown in Fig. 6, *mDom*$^{fl/fl}$*;CreER* cells expressing mDomino-HA displayed normal proliferation, cell-cycle distribution, and nuclear morphology irrespective of the OHT-induced deletion of the endogenous mDomino. This showed that the cell-cycle deficiency could be rescued by the exogenous expression of the wild-type mDomino protein and was, therefore, due to the absence of mDomino.

Impairment of Cell-cycle Regulatory Gene Expression in mDomino-deficient Cells—The p400/mDomino chromatin-remodeling complex is known to interact physically or functionally with cell-cycle-regulatory transcription factors, including c-Myc, E1A, p53, and E2F (3, 17–20). To gain insight into the molecular function of mDomino in cell-cycle regulation, we characterized the gene expression profiles of *mDom*$^{fl/fl}$*;CreER* MEFs treated or untreated with OHT by DNA microarray analysis (n = 3 for both untreated and OHT-treated cells), which revealed that 770 genes were differentially (≥2.0-fold) expressed by mDomino depletion, including 191 down-regulated genes (supplemental Table 1) and 579 up-regulated genes (data not shown). A gene annotation analysis revealed that, among the 93 genes whose expression was reduced to <45% by OHT treatment, many (27 genes) are characterized as cell-cycle-related genes, such as *E2F2*, *E2F7*, *E2F8*, *CENP-F* (*cenpf*), *Skp2*, *Nek2*, and *Cyclin A2* (*ccna2*) (Table 1). Moreover, 17 of the 93 genes are known Myc targets (supplemental Table 1) (Myc Cancer Gene, available on-line).

To confirm the microarray data and to characterize the time course of mRNA expression during cell-cycle progression, we carried out quantitative RT-PCR analysis of the genes for *Skp2*, *PLK1*, *CENP-F*, and *FoxM1*. As reported previously, the expressions of these genes were dependent on cell-cycle progression in the control *mDom*$^{fl/fl}$*;CreER* MEFs (Fig. 7*A*). In cells treated with OHT, the expression levels of these genes were low, and they were not clearly induced after the serum stimulation. We have also compared expression of *c-Myc*, *E2F1*, *p53*, and *H2A.Z* genes in the OHT-treated or -untreated cells. Expression levels of *p53* and *H2A.Z* in the mDomino-deleted cells were consis-

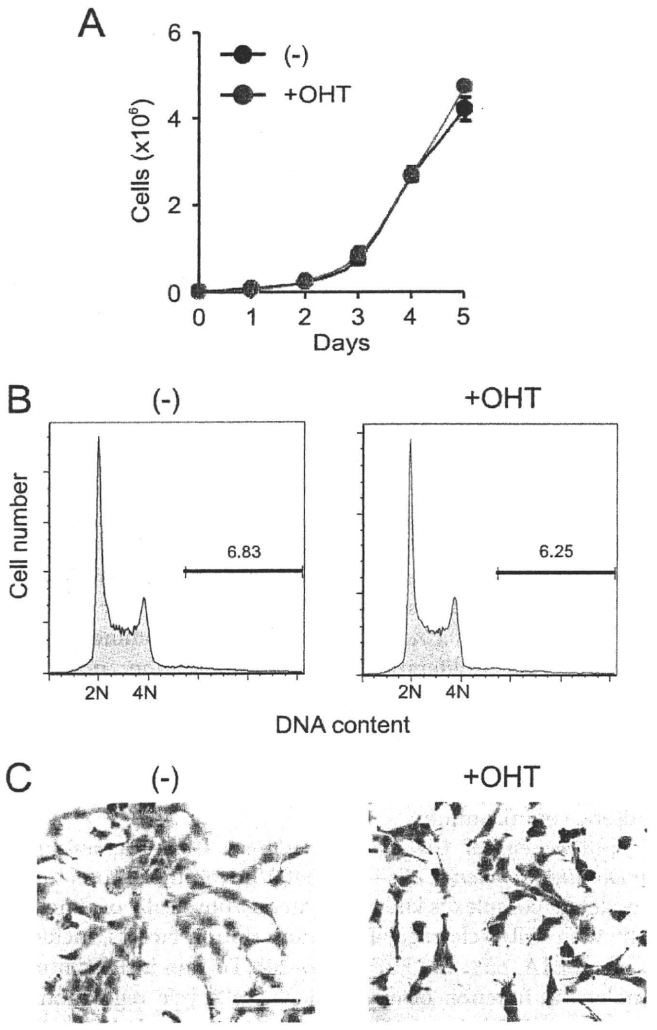

FIGURE 6. **Rescue of the cell-cycle phenotype by the exogenous expression of mDomino cDNA.** *mDom$^{fl/fl}$;CreER* MEFs were transfected with an mDomino expression plasmid, and stable transformants were cultured with or without OHT treatment. *A*, growth curve of the transformant MEFs treated with (+) or without (−) OHT. Data are the means ± S.D. of three separate experiments. *B*, cell-cycle profiles of the transformants treated without or with OHT and then cultured for 6 days. *C*, Wright-Giemsa staining of the transformants grown as in *B*. *Scale bars* represent 100 μm.

TABLE 1
Cell-cycle-related genes affected by mDomino deletion

DNA microarray analysis of OHT-treated (+OHT) or untreated (−) *mDom$^{fl/fl}$;CreER* MEFs were performed as described under "Experimental Procedures." Among the 93 genes whose expression was reduced to <45% by OHT treatment (supplemental Table 1), genes that are characterized as "cell cycle" are listed.

Gene symbol	-fold change	+OHT	(−)	*p* value	Accession number
E2f2	3.5	30	107	7.33E-05	BB543028
Mybl2	3.2	208	666	2.42E-04	NM_008652
Cenpf	3.2	97	310	1.02E-02	BB667318
Psrc1	3.0	288	878	4.66E-04	NM_019976
Fbxo5	3.0	618	1851	7.31E-05	AK011820
E2f7	2.7	557	1517	3.98E-03	BG069355
Cdc6	2.7	564	1531	4.25E-05	NM_011799
Ccna2	2.6	2615	6868	2.04E-03	X75483
Ccnf	2.6	144	378	3.59E-03	BB089717
Rbl1	2.6	178	465	2.64E-04	U27178
E2f8	2.6	336	876	2.80E-05	BM247465
Rcc1	2.6	470	1213	5.99E-06	NM_133878
2810433K01Rik	2.5	581	1461	2.32E-04	NM_025581
Mapk12	2.5	134	336	6.35E-04	BC021640
Cdca3	2.5	1732	4277	1.52E-03	BI081061
Uhrf1	2.4	192	470	6.75E-03	BB702754
Suv39h2	2.4	353	854	7.45E-04	NM_022724
Plk1	2.4	742	1787	3.42E-05	NM_011121
Rassf1	2.4	83	198	2.07E-03	BB385028
Cdc25a	2.4	590	1405	1.46E-02	C76119
Nek2	2.4	339	802	3.80E-04	NM_010892
Skp2	2.3	221	518	1.43E-02	AV259620
Sgol1	2.3	314	732	3.92E-03	BB410537
Incenp	2.3	87	201	2.06E-04	AV301185
Mcm3	2.3	234	531	1.02E-03	BI658327
Cdc20	2.2	2367	5311	3.80E-03	NM_023223
Ncapg2	2.2	1610	3593	1.26E-03	NM_133762

tently lower than those in the untreated cells. Unexpectedly, the expression of *c-Myc* and *E2F1* genes was rather up-regulated in the mDomino-deficient MEFs (Fig. 7*B*), suggesting that mDomino may be involved in repression of these genes by a direct mechanism or by an indirect, feedback pathway. RT-PCR analysis of the mDomino mRNA showed that the expression of mDomino in normal cells was independent of the cell cycle (supplemental Fig. 2). Finally, we examined whether the impaired expression of the cell-cycle-related genes could be rescued by the exogenous expression of mDomino protein. The *mDom$^{fl/fl}$;CreER* MEFs expressing mDomino-HA exhibited a normal expression of the cell-cycle-regulated genes irrespective of OHT treatment (Fig. 7*C*). In contrast, the expression of c-Myc, which was up-regulated in the mDom-deficient cells, was reduced to normal by the mDomino expression (Fig. 7*D*). Together, these results indicated that mDomino plays an essential role in the expression of various genes that are involved in cell-cycle regulation and suggested that the impaired expression of those genes causes the aberrant cell-cycle progression, growth arrest, and mitotic catastrophe of the mDomino-deficient cells.

DISCUSSION

In this report, we generated conditional knock-out mice of the p400/mDomino gene. These mice died within 2 weeks of pI:pC-induced, Mx1-Cre-mediated mDomino depletion. We showed that the mDomino deletion in BM cells resulted in the rapid loss of committed myeloid and erythroid cells as well as hematopoietic progenitor/stem cells. The extinction of hematopoietic cells from the BM was probably due to both a decrease in the proliferation and an increase in the apoptotic cell death of the mDomino-deleted cells, followed by their clearance and replacement by mature erythrocytes. A hematopoietic colony formation assay demonstrated that the IFN-induced deletion of mDomino strongly inhibited the growth of all the colony-forming progenitors, including the myeloid, erythroid, and megakaryocytic lineages, suggesting that the impaired hematopoiesis was cell autonomous and not caused by a defect in the hematopoiesis-supporting environment in the BM.

The strong growth inhibition of the mDomino-deficient hematopoietic cells prompted us to investigate the cell proliferation using embryonic fibroblasts from *mDom$^{fl/fl}$* mice. The induced deletion of the mDomino gene led to an acute and strong inhibition of the cellular proliferation of MEFs. Cell-cycle analysis revealed that the mDomino-deficient MEFs exhibited pleiotropic cell-cycle defects, including delayed and insufficient entry into the S phase, increase in the G_2/M phase,

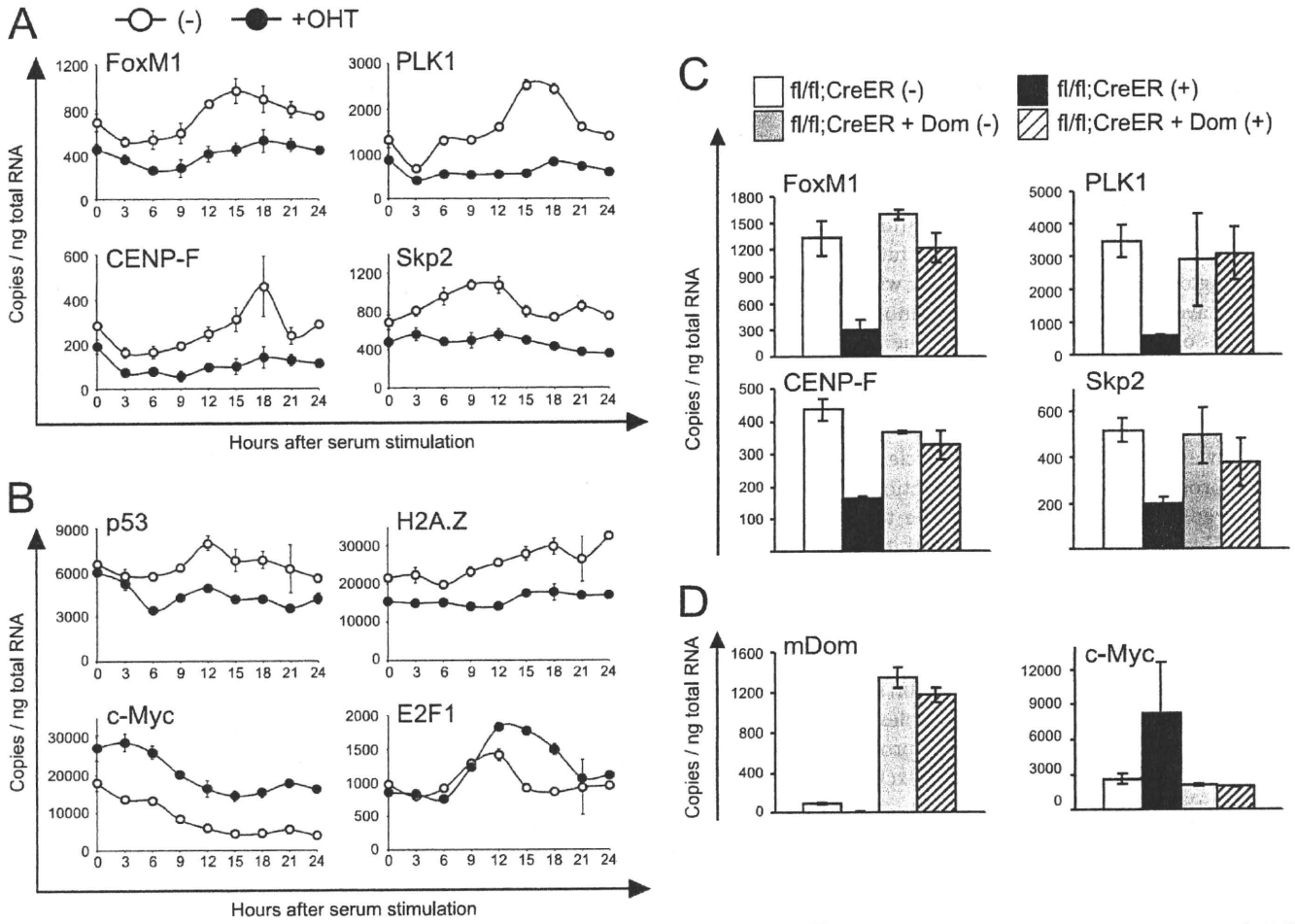

FIGURE 7. **Expression of cell-cycle-related genes in mDomino-deleted MEFs.** *A* and *B*, *mDom*$^{fl/fl}$*;CreER* MEFs were untreated (−) or treated (+) with OHT, serum-starved for 24 h, and then re-stimulated with 10% fetal bovine serum. At the indicated times, the RNA was extracted and analyzed for expression of the indicated genes by quantitative RT-PCR. *C* and *D*, parental *mDom*$^{fl/fl}$*;CreER* MEFs and mDomino-expressing transformants (*fl/fl;CreER + Dom*) were untreated (−) or treated (+) with OHT, cultured for 3 days, and then subjected to expression analysis by quantitative RT-PCR.

and the accumulation of polyploid and/or multinucleated cells with micronuclei. These phenotypes are very similar to those of *Trrap*-deleted MEFs, in which a spindle checkpoint failure leads to mitotic catastrophe (33), suggesting that the polyploid and/or multinucleated population of mDom-deficient cells might arise from a failure in mitotic checkpoint followed by endoreduplication of the DNA without cytokinesis. In *Saccharomyces cerevisiae*, the Swr1 complex is involved in chromosome segregation and plays an important role in chromosome stability (34). In addition, the TRRAP-Tip60 complex, which also contains p400/mDomino, is known to be required for the recruitment and accumulation of DNA repair proteins at sites of DNA double-strand break (35). Thus, p400/mDomino may also be involved in maintaining chromosome integrity.

In the human osteosarcoma U2OS cell line and primary fibroblasts, the shRNA-mediated knockdown of p400/mDomino results in the induction of cell-cycle inhibitor p21, cell-cycle arrest at G_1, and premature senescence (21, 22). However, the mDomino-deleted MEFs, which also showed strong growth inhibition, did not show up-regulated *p21* expression (data not shown), suggesting that the loss of mDomino can block the cell cycle by a mechanism other than the p53-p21 pathway. Our DNA microarray analysis showed that the expression levels of many cell-cycle-related genes were significantly reduced in the mDomino-deleted MEFs. Interestingly, among the strongly affected genes, *CENP-F*, *Nek2*, and *Plk1* are representative G_2/M-specific genes that are regulated by the transcription factor FoxM1 (36–38), which was also among the strongly reduced genes. This finding indicates that the cell-cycle phenotypes of the mDomino-deficient MEFs were at least partly due to the impaired expression of FoxM1 and its target genes. In this regard, it is noteworthy that *FoxM1*-deficient MEFs exhibit mitotic malfunction similar to our results (36). However, the exogenous overexpression of FoxM1 cDNA in *mDom*$^{fl/fl}$*;CreER* MEFs failed to rescue the cell-cycle phenotype (data not shown), suggesting that p400/mDomino is responsible for the regulated expression not only of FoxM1 targets but also of other cell-cycle-related genes. A candidate transcription factor of note is the oncoprotein c-Myc, which interacts with the Tip60-TRRAP-p400/mDomino complex and regulates the expression of various genes positively or negatively, possibly through the histone-acetyl-transferring and/or the H2A.Z-exchanging activities of the complex (3, 17, 19). This hypothesis is consistent with the results of our microarray analysis

(supplemental Table 1), in which the strongly affected genes included several Myc targets, such as *E2F2*, *Mybl2*, *Cdc6*, *Cyclin A*, and *FoxM1* (39–43). To elucidate whether p400/mDomino is directly involved in the regulatory expression of these genes, we need to investigate physical and functional interactions of the p400/mDomino chromatin-remodeling complex with the c-Myc and/or FoxM1 on the promoter region of their target genes by chromatin immunoprecipitation analyses using cell-cycle-synchronized fibroblasts, in our future experiments.

Taking our present results together with our previous studies, we have shown that p400/mDomino is essential for hematopoiesis of both the yolk sac and the adult BM. The acute extinction of hematopoietic cells is probably due to the strong growth inhibition and apoptotic cell death of the mDomino-deleted cells. We also provide evidence that p400/mDomino plays an essential role in the cell-cycle progression of fibroblasts, probably through its transcriptional activation of cell-cycle-regulatory genes, especially the targets of FoxM1 and c-Myc. Because p400/mDomino exerts its chromatin-remodeling function via its H2A.Z-exchange activity, the interaction of p400/mDomino with c-Myc (and possibly with FoxM1) might regulate the deposition and/or eviction of the H2A.Z variant at the promoter nucleosome of cell-cycle-regulatory genes (14, 16, 44). Future studies on the interaction between transcription factors and the p400/mDomino complex and their role in the H2A.Z-positioning mechanism will provide insight into the biological significance of the H2A.Z-exchanging machinery in cell growth and differentiation.

Acknowledgments—We are grateful to Dr. Shigeyoshi Itohara and the RIKEN BioResource Center for providing the FLPe transgenic mice. We also thank Dr. Toru Nakano for the Cre-ER^{T2} construct, and Dr. Joe S. Mymryk for the E1A cDNAs.

REFERENCES

1. Saha, A., Wittmeyer, J., and Cairns, B. R. (2006) *Nat. Rev. Mol. Cell Biol.* **7,** 437–447
2. Cairns, B. R. (2007) *Nat. Struct. Mol. Biol.* **14,** 989–996
3. Fuchs, M., Gerber, J., Drapkin, R., Sif, S., Ikura, T., Ogryzko, V., Lane, W. S., Nakatani, Y., and Livingston, D. M. (2001) *Cell* **106,** 297–307
4. Ogawa, H., Ueda, T., Aoyama, T., Aronheim, A., Nagata, S., and Fukunaga, R. (2003) *Genes Cells* **8,** 325–339
5. Kobor, M. S., Venkatasubrahmanyam, S., Meneghini, M. D., Gin, J. W., Jennings, J. L., Link, A. J., Madhani, H. D., and Rine, J. (2004) *PLoS Biol.* **2,** E131
6. Ruhf, M. L., Braun, A., Papoulas, O., Tamkun, J. W., Randsholt, N., and Meister, M. (2001) *Development* **128,** 1429–1441
7. Cai, Y., Jin, J., Florens, L., Swanson, S. K., Kusch, T., Li, B., Workman, J. L., Washburn, M. P., Conaway, R. C., and Conaway, J. W. (2005) *J. Biol. Chem.* **280,** 13665–13670
8. Jin, J., Cai, Y., Yao, T., Gottschalk, A. J., Florens, L., Swanson, S. K., Gutiérrez, J. L., Coleman, M. K., Workman, J. L., Mushegian, A., Washburn, M. P., Conaway, R. C., and Conaway, J. W. (2005) *J. Biol. Chem.* **280,** 41207–41212
9. Krogan, N. J., Keogh, M. C., Datta, N., Sawa, C., Ryan, O. W., Ding, H., Haw, R. A., Pootoolal, J., Tong, A., Canadien, V., Richards, D. P., Wu, X., Emili, A., Hughes, T. R., Buratowski, S., and Greenblatt, J. F. (2003) *Mol. Cell* **12,** 1565–1576
10. Mizuguchi, G., Shen, X., Landry, J., Wu, W. H., Sen, S., and Wu, C. (2004) *Science* **303,** 343–348
11. Kusch, T., Florens, L., Macdonald, W. H., Swanson, S. K., Glaser, R. L., Yates, J. R., 3rd, Abmayr, S. M., Washburn, M. P., and Workman, J. L. (2004) *Science* **306,** 2084–2087
12. Jin, J., Cai, Y., Li, B., Conaway, R. C., Workman, J. L., Conaway, J. W., and Kusch, T. (2005) *Trends Biochem. Sci.* **30,** 680–687
13. van Attikum, H., and Gasser, S. M. (2005) *Nat. Rev. Mol. Cell Biol.* **6,** 757–765
14. Squatrito, M., Gorrini, C., and Amati, B. (2006) *Trends Cell Biol.* **16,** 433–442
15. Morrison, A. J., and Shen, X. (2009) *Nat. Rev. Mol. Cell Biol.* **10,** 373–384
16. Svotelis, A., Gévry, N., and Gaudreau, L. (2009) *Biochem. Cell Biol.* **87,** 179–188
17. Frank, S. R., Parisi, T., Taubert, S., Fernandez, P., Fuchs, M., Chan, H. M., Livingston, D. M., and Amati, B. (2003) *EMBO Rep.* **4,** 575–580
18. Taubert, S., Gorrini, C., Frank, S. R., Parisi, T., Fuchs, M., Chan, H. M., Livingston, D. M., and Amati, B. (2004) *Mol. Cell. Biol.* **24,** 4546–4556
19. Gévry, N., Chan, H. M., Laflamme, L., Livingston, D. M., and Gaudreau, L. (2007) *Genes Dev.* **21,** 1869–1881
20. Lu, J., Ruhf, M. L., Perrimon, N., and Leder, P. (2007) *Proc. Natl. Acad. Sci. U.S.A.* **104,** 9381–9386
21. Chan, H. M., Narita, M., Lowe, S. W., and Livingston, D. M. (2005) *Genes Dev.* **19,** 196–201
22. Tyteca, S., Vandromme, M., Legube, G., Chevillard-Briet, M., and Trouche, D. (2006) *EMBO J.* **25,** 1680–1689
23. Fazzio, T. G., Huff, J. T., and Panning, B. (2008) *Cell* **134,** 162–174
24. Ueda, T., Watanabe-Fukunaga, R., Ogawa, H., Fukuyama, H., Higashi, Y., Nagata, S., and Fukunaga, R. (2007) *Genes Cells* **12,** 581–592
25. Kanki, H., Suzuki, H., and Itohara, S. (2006) *Exp. Anim.* **55,** 137–141
26. Williams-Simons, L., and Westphal, H. (1999) *Transgenic Res.* **8,** 53–54
27. Kühn, R., Schwenk, F., Aguet, M., and Rajewsky, K. (1995) *Science* **269,** 1427–1429
28. Ueda, T., Watanabe-Fukunaga, R., Fukuyama, H., Nagata, S., and Fukunaga, R. (2004) *Mol. Cell. Biol.* **24,** 6539–6549
29. Weischenfeldt, J., Damgaard, I., Bryder, D., Theilgaard-Mönch, K., Thoren, L. A., Nielsen, F. C., Jacobsen, S. E., Nerlov, C., and Porse, B. T. (2008) *Genes Dev.* **22,** 1381–1396
30. Morita, S., Kojima, T., and Kitamura, T. (2000) *Gene Ther.* **7,** 1063–1066
31. Iida, S., Kohro, T., Kodama, T., Nagata, S., and Fukunaga, R. (2005) *J. Leukoc. Biol.* **78,** 481–490
32. Feil, R., Wagner, J., Metzger, D., and Chambon, P. (1997) *Biochem. Biophys. Res. Commun.* **237,** 752–757
33. Herceg, Z., Hulla, W., Gell, D., Cuenin, C., Lleonart, M., Jackson, S., and Wang, Z. Q. (2001) *Nat. Genet.* **29,** 206–211
34. Krogan, N. J., Baetz, K., Keogh, M. C., Datta, N., Sawa, C., Kwok, T. C., Thompson, N. J., Davey, M. G., Pootoolal, J., Hughes, T. R., Emili, A., Buratowski, S., Hieter, P., and Greenblatt, J. F. (2004) *Proc. Natl. Acad. Sci. U.S.A.* **101,** 13513–13518
35. Murr, R., Loizou, J. I., Yang, Y. G., Cuenin, C., Li, H., Wang, Z. Q., and Herceg, Z. (2006) *Nat. Cell Biol.* **8,** 91–99
36. Laoukili, J., Kooistra, M. R., Brás, A., Kauw, J., Kerkhoven, R. M., Morrison, A., Clevers, H., and Medema, R. H. (2005) *Nat. Cell Biol.* **7,** 126–136
37. Laoukili, J., Stahl, M., and Medema, R. H. (2007) *Biochim. Biophys. Acta* **1775,** 92–102
38. Fu, Z., Malureanu, L., Huang, J., Wang, W., Li, H., van Deursen, J. M., Tindal, D. J., and Chen, J. (2008) *Nat. Cell Biol.* **10,** 1076–1082
39. Menssen, A., and Hermeking, H. (2002) *Proc. Natl. Acad. Sci. U.S.A.* **99,** 6274–6279
40. Fernandez, P. C., Frank, S. R., Wang, L., Schroeder, M., Liu, S., Greene, J., Cocito, A., and Amati, B. (2003) *Genes Dev.* **17,** 1115–1129
41. Li, Z., Van Calcar, S., Qu, C., Cavenee, W. K., Zhang, M. Q., and Ren, B. (2003) *Proc. Natl. Acad. Sci. U.S.A.* **100,** 8164–8169
42. Menssen, A., Epanchintsev, A., Lodygin, D., Rezaei, N., Jung, P., Verdoodt, B., Diebold, J., and Hermeking, H. (2007) *Cell Cycle* **6,** 339–352
43. Herold, S., Herkert, B., and Eilers, M. (2009) *Nat. Rev. Cancer* **9,** 441–444
44. Martinato, F., Cesaroni, M., Amati, B., and Guccione, E. (2008) *PLoS One* **3,** e3650

Phytomedicine 17 (2010) 170–177

Contents lists available at ScienceDirect

Phytomedicine

journal homepage: www.elsevier.de/phymed

The fixed herbal drug composition "Saikokaryukotsuboreito" prevents bone loss with an association of serum IL-6 reductions in ovariectomized mice model ☆

T. Hattori [a,*], W. Fei [b], T. Kizawa [a], S. Nishida [b], H. Yoshikawa [a], Y. Kishida [b]

[a] Department of Orthopaedics, Osaka University Graduate School of Medicine, 2-2 Yamadaoka, Suita, Osaka 565-0871, Japan
[b] Department of Kampo Medicine, Osaka University Graduate School of Medicine, Osaka, Japan

ARTICLE INFO

Keywords:
Saikokaryukotsuboreito
Osteoporosis
IL-6
Herbal medicine

ABSTRACT

Purpose: Saikokaryukotsuboreito (SRB) is a traditional Japanese herbal medicine that has been used to treat hyperlipidemia. As some studies have shown that lipid-lowering drugs reduce osteoporosis, we investigated the effect of SRB on bone metabolism in the postmenopausal period using an ovariectomized (OVX) murine model.

Material and Methods: Fifteen aged 9 weeks female mice were divided into three groups ($n=5$ each). The OVX group and SRB group underwent bilateral ovariectomy, after which the OVX group was fed a normal diet and the SRB group fed a normal diet containing 2% SRB. The sham group underwent sham surgery and was then fed a normal diet. Eight weeks after surgery, all mice were sacrificed, and bone volume, bone histomorphometric parameters, and bone-associated phenotype were compared among the groups.

Results: Compared with the OVX group, the SRB group showed suppression of bone volume loss at the tibia (SRB group: $12.7 \pm 0.7\%$, OVX group: $9.8 \pm 0.4\%$; $p=0.005$, ANOVA) and lumbar spine (SRB group: $15.1 \pm 0.9\%$, OVX group: $11.3 \pm 0.1\%$; $p=0.031$, ANOVA). A significant decrease in eroded surface was also observed in SRB-treated ovariectomized mice compared with the OVX group ($p=0.022$, ANOVA). We also found that serum levels of interleukin (IL)-6, a primary mediator of bone resorption, in the SRB group were significantly lower than in the OVX group (SRB: 52.5 ± 6.8 pg/ml; OVX: 138.0 ± 23.1 pg/ml; $p=0.011$, ANOVA). However, unexpectedly, SRB did not affect estradiol and total cholesterol in ovariectomized mice.

Conclusion: SRB can prevent loss of bone volume and suppress serum IL-6 levels in this postmenopausal model and is a promising candidate for treatment of postmenopausal osteoporosis.

Introduction

Postmenopausal osteoporosis is one of the natural consequences of aging (Riggs and Melton, 1995). It is a skeletal disorder characterized by progressive loss of bone tissue and deterioration of osseous microarchitecture which begins after natural or surgical menopause and results in an increased risk of fracture (Hodsman, 2001). Melton et al. (1989) reported that 25% of women aged 80–84 years have had at least one vertebral fracture. Fractures can reduce mobility and be very painful, thereby limiting everyday activities (Hill, 1996).

Epidemiological evidence has accumulated indicating that osteoporosis and hyperlipidemia frequently coexist, suggesting a link between bone and lipid metabolism (Ray et al., 2002). Several studies have shown that statins, which are known to have lipid-lowering effects, also have potentially beneficial effects on bone metabolism (Edwards et al., 2000; Mundy et al., 1999).

Saikokaryukotsuboreito (SRB) (Tsumura Co., Tokyo, Japan) is a traditional Japanese herbal medicine that has been used to decrease serum triglycerides and inhibit aortic intimal thickening in hypertension (Yamada et al., 1998).

This study investigated the effects of SRB on bone morphology and substances associated with bone metabolism in the postmenopausal period using an ovariectomized mouse model.

☆ This study was supported in part by grants from the Ministry of Education, Science, Sports and Culture, Japan (# 19791029 [Y. K.]).

* Corresponding author. Tel.: +81 06 6879 3552; fax: +81 06 6879 3559.
E-mail address: takako-hattori@umin.ac.jp (T. Hattori).

0944-7113/$ - see front matter © 2010 Elsevier GmbH. All rights reserved.
doi:10.1016/j.phymed.2009.12.004

Materials and methods

Preparation of SRB extract, three-dimensional HPLC analysis and liquid chromatography-mass spectrometry (LC-MS/MS)

The SRB extract used was manufactured by Tsumura & Co. (Tokyo, Japan). It is composed of 10 crude drugs in fixed proportions: 5.0 g of Bupleurum Root (the root of *Bupleurum falcatum* Linne), 4.0 g of Pinelliae Tuber (the tuber of *Pinellia ternate* Breitenbach), 3.0 g of Cinnamon Bark (the bark of *Cinnamomum cassia* Blume), 3.0 g of Poria Sclerotium (the sclerotium of *Poria cocos* Wolf), 2.5 g of Scutellariae Root (the root of *Scutellaria baicalensis* Georgi), 2.5 g of Jujube (the fruit of *Zizyphus jujube* Miller var. *inermis* Rehder), 2.5 g of Ginseng (the root of *Panax ginseng* C. A. Meyer), 2.5 g of Ostreae Shell (the shell of *Ostrea gigas* Thunberg), 2.5 g of Longgu (the *Fossilia ossis mastodi*, mainly comprising calcium carbonate), and 1.0 g of Ginger (the rhizome of *Zingiber officinal* Roscoe). These crude drugs were decocted in a 10-fold volume of water for 60 min, filtered, and the filtrate spray-dried to obtain an extract yield of about 10% by weight of the original preparation. For the analysis of SRB components, the aqueous extract (0.5 g) was extracted with 20 ml of methanol under ultrasonication for 30 min. The solution was filtered through a membrane filter (0.45 μn) then subjected to high-performance liquid chromatography (HPLC) analysis. The HPLC apparatus consisted of a Shimadzu LC 10A (analysis system software: CLASS-M10A ver. 1.64, Tokyo, Japan) equipped with a multiple wavelength detector (UV 200–400 nm) (Shimadzu SPD-M10AVP, diode array detector) and an auto injector (Shimadzu CTO-10AC). HPLC conditions were as follows: column, ODS (TSK-GEL 80TS, 250 × 4.6 mm i.d., TOSOH, Tokyo, Japan); eluant, (A) 0.05 M $AcONH_4$ (pH 3.6), (B) 100% CH_3CN; linear gradient of 90% A and 10% B changing to 0% A and 100% B in 60 min (100% B was continued for 20 min); temperature, 40 °C; flow rate, 1.0 ml/min. The HPLC profile of SRB extract is shown in Fig. l. Baicalin, baicalein, oroxylin-A and wogonin were detected as the major compounds of SRB, while cinnamic acid, saikosaponin, gingerol, and cinnamaldehyde were also observed. However, we could not detect ginsenoside, pachymic acid and beturinic acid in this HPLC analysis. Thus, we performed LC-MS/MS analysis (Fig. 2A) of Fr.1 using a system with the 1100 Agilent auto sampler, HPLC instrument (Agilent Technologies, Inc. Tokyo, Japan), and API 2000 mass spectrometer (Applied Biosystems/MDS Sciex, Tokyo, Japan). Chromatography was carried out on a reversed-phase YMC Pack ODS-AQ column (50 × 2.0 mm i.d.) with the mobile phase consisting of solvent A (10 mM ammonium formate) and solvent B (acetonitrile). A 22-min gradient was established running from 23% to 35% B over the first 4 min, 35% to 90% B over the following 5 min, and 90% B over the last 3 min before returning the system to its initial 23% B at 10 min. For qualification, Fr.1 was prepared in methanol, filtered, and transferred to the auto sampler for LC-MS/MS analysis. Standards were prepared in a mixture of methanol, 10 mM ammonium formate and acetonitrile (3:3:2). Standards and Fr.1 were injected (10 μl) into the LC-MS/MS system.

The column effluent was introduced into the mass spectrometer using electrospray ionization (ESI) in the positive and negative ion modes with nitrogen as the nebulizer and curtain gas. In the positive ion mode, the nebulizer current and temperature were 40 psi and 450 °C, respectively. The collision gas (N_2) was set at 5 psi and collision energy was 17 eV (pachymic acid), 29 eV (ginsenoside Rg1), 29 eV (ginsenoside Rf), 35 eV (ginsenoside Re), 43 eV (ginsenoside Rc), 47 eV (ginsenoside Rb1), and 43 eV (ginsenoside Rb2) with an electron multiplier voltage of

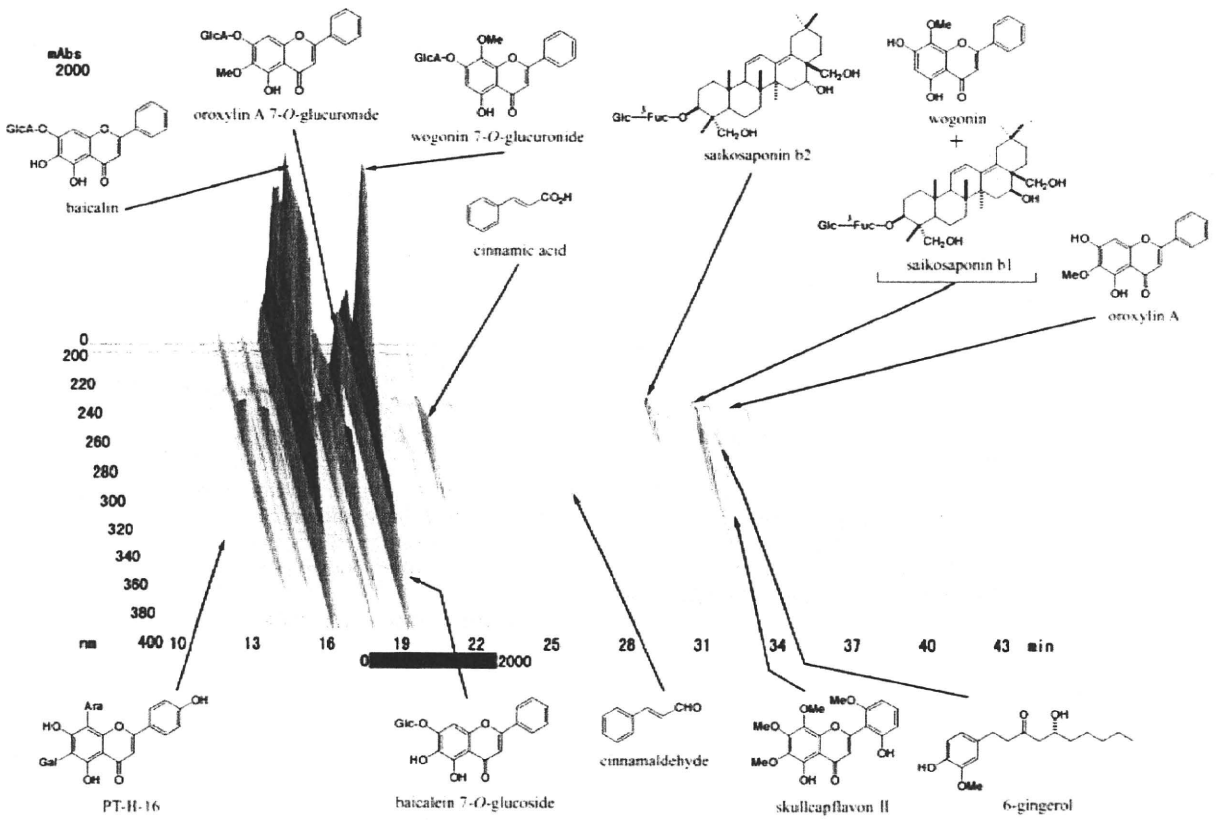

Fig. 1. Three-dimensional high performance liquid chromatography profile of SRB.

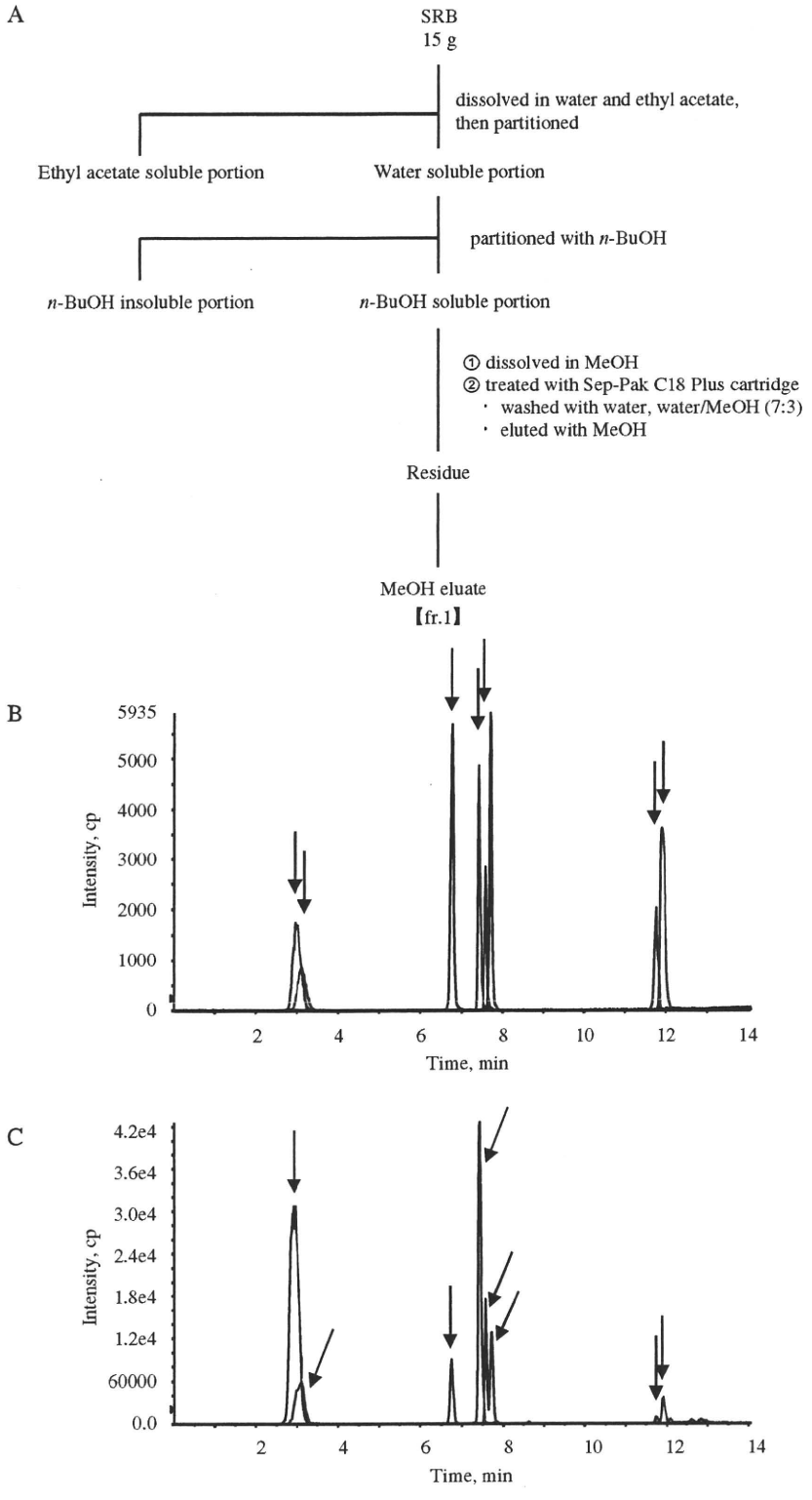

Fig. 2. Liquid chromatography-mass spectrometry profile of SRB. (A) The schema of this analysis. (B) Standard solution. Retention times (min); 2.97 (ginsenoside Rg1), 3.11 (ginsenoside Re), 6.78 (ginsenoside Rf), 7.43 (ginsenoside Rb1), 7.58 (ginsenoside Rc), 7.71 (ginsenoside Rb2), 11.77 (pachymic acid), 11.91 (betulinic acid). (C) A methanolic solution of Fr. 1. Retention times (min); 2.92 (ginsenoside Rg1), 3.10 (ginsenoside Re), 6.75 (ginsenoside Rf), 7.42 (ginsenoside Rb1), 7.57 (ginsenoside Rc), 7.72 (ginsenoside Rb2), 11.78 (pachymic acid), 11.92 (betulinic acid).

5500 V. Ginsenoside analog ions were detected as ammonium adducts [M+NH4+]+. In the negative ion mode, the nebulizer current and temperature were 20 psi and 450 °C, respectively. The collision gas (N_2) was set at 2 psi and collision energy was −24 eV (beturinic acid) with an electron multiplier voltage of −4200 V. Betulinic acid ion was detected as formate adducts

[M+HCOO−]−.The following mass transitions were used for MRM analysis: pachymic acid m/z=529/511, ginsenoside Rg1 m/z=818/423, ginsenoside Rf m/z=818/423, ginsenoside Re m/z=965/423, ginsenoside Rc m/z=1097/325, ginsenoside Rb1 m/z-1127/325, ginsenoside Rb2 m/z=1097/325 (positive ion mode), and betulinic acid m/z=501/455 (negative ion mode) (Fig. 2B and C). The LC-MS/MS system was controlled by BioAnalyst 1.4.1 software.

SRB preparation and animals

Spray-dried, water-extracted SRB powder was obtained from Tsumura & Co. C57BL/6N female mice, aged 8 weeks, were purchased from Japan Oriental Yeast Co. (Tokyo, Japan). All mice were housed under specific pathogen-free conditions with a 12 h light/dark cycle. The housing care rules and experimental protocol were approved by the Animal Care and Use Committee of Osaka University.

At the age of 9 weeks, these mice, with an average body weight 19.8 g (19.8 ± 0.3 g), were randomly divided into three groups. The first group (OVX group, n=5) and the second group (SRB group, n=5) were anesthetized with intraperitoneal injection of pentobarbital (Dainippon Sumitomo Pharma, Osaka, Japan) and bilaterally ovariectomized. For 8 weeks after surgery, the OVX group was fed a normal diet (powdered MF, Oriental Yeast Co., Ltd) and the SRB group was fed a normal diet containing 2% SRB. The last group (sham group, n=5) was sham-operated and fed a normal diet for 8 weeks after surgery. General condition, food intake, and body weight were recorded for all mice.

Micro-computed tomography (CT)

Eight weeks after surgery, at 17 weeks old, all mice were sacrificed. The tibia from each animal was sampled and the soft tissue cleaned off. The proximal metaphysis of the tibia was then scanned with a Micro-CT system (SMX-100CT-SV; Shimadzu, Kyoto, Japan) in 600 slices at a tube voltage of 45 kV and tube current of 75 μA, and the trabecular bone area (percentage of bone volume [BV] per tissue volume [TV]) was measured.

Bone histomorphometry

All mice were injected subcutaneously with 16 mg/kg calcein 7 and 2 days before being sacrificed. The lumbar spine was removed and fixed with 70% ethanol, dehydrated, and embedded in glycolmethacrylate (GMA) resin. The region studied was the secondary spongiosa, excluding the primary spongiosa 0.2 mm distal from the growth plate. Static and dynamic bone histomorphometric measurements of trabecular bone area were performed. Bone histomorphometric parameters were measured as described in the report of The American Society for Bone and Mineral Research (ASBMR) Histomorphometry Nomenclature Committee (Perfitt et al., 1987).

Serum analysis

Immediately after sacrifice, blood was withdrawn from the abdominal aorta. Serum estradiol and interleukin (IL)-6 levels were measured using an enzyme-linked immunoassay kit (estradiol: Cayman Chemical, Ann Arbor, MI, USA; IL-6: Bender Medsystems, Vienna, Austria). Total cholesterol was measured using a Wako L-type CHO H kit (Wako Pure Chemical Industries, Osaka, Japan). Sensitivities of these assays were as follows: estradiol, 20 pg/ml; total cholesterol, 0.4 mg/dl; IL-6, 12 pg/ml.

Statistical analysis

All data are expressed as the mean ± standard error of the mean (SEM). Statistical analysis was performed using JMP IN 5.1 (SAS Institute, Cary, NC, USA). Statistical significance of comparisons was determined by one-way analysis of variance (ANOVA). Values of $p < 0.05$ were considered to indicate statistical significance.

Results

SRB had no adverse effects

All mice survived after ovariectomy or sham operation. No mice in the SRB group experienced side effects, including weight loss or unusual activity. There was no significant difference in food intake per day among the three groups (OVX: 4.1 ± 1.1 g; SRB: 4.0 ± 0.8 g; sham: 3.5 ± 0.3 g; one-way ANOVA, p=0.16). There was also no significant difference in body weight among the three groups (OVX: 29.8 ± 0.4 g; SRB: 29.5 ± 0.8 g; sham: 28.1 ± 0.5 g; one-way ANOVA, p=0.14) at the end of the experiment.

SRB suppressed loss of tibial trabecular bone volume in ovariectomized mice

To investigate the role of SRB in bone metabolism, we determined structural changes in trabecular bone with micro-CT. Fig. 3A–C show representative micro-CT images of the proximal tibia of the three groups, indicating deterioration of the microarchitecture in the OVX group compared with the SRB group. Fig. 3D shows that trabecular bone volume in the SRB group was significantly greater than in the OVX group (OVX group: 9.8 ± 0.4%; SRB group: 12.7 ± 0.7%; sham group: 17.2 ± 1.2% one-way ANOVA, p=0.0001). Although the differences between the SRB and sham group were statistically significant, bone volume in the SRB group tend to be maintained closer to levels in the sham group compared with the OVX group.

SRB suppressed loss of trabecular bone volume of lumbar vertebrae in ovariectomized mice

Bone histomorphometric parameters at the end of the experiment are shown in Fig. 4. Bone volume of the lumbar vertebrae was significantly larger in the SRB group than in the OVX group (one-way ANOVA, p=0.0015, Fig. 4A). Bone volume in the SRB group did not differ significantly from that in the sham group. Trabecular bone number (Tb.N) and trabecular bone space (Tb.Sp) in the SRB group were closer to sham group readings than those in the OVX group, although the differences between the SRB and sham group were statistically significant (Tb.N, one-way ANOVA, p=0.0014; Tb.Sp, p=0.0008; Fig. 4C and D).

The ratios of osteoblast surface (Ob.S)/bone surface (BS) and osteoclast surface (Oc.S)/BS in the SRB group tended to be smaller than those in the OVX group, but there were no significant differences between these two groups (Ob.S/BS: one-way ANOVA, p=0.81; Oc.S/BS: p=0.29; Fig. 4E and H).

The eroded surface (ES)/BS (%) was significantly smaller in the SRB group than in the OVX group (one-way ANOVA, p=0.054, Fig. 4F). No significant difference was observed between the SRB and OVX groups for mineral apposition rate (MAR) or bone formation rate (BFR) (Fig. 4I and K).

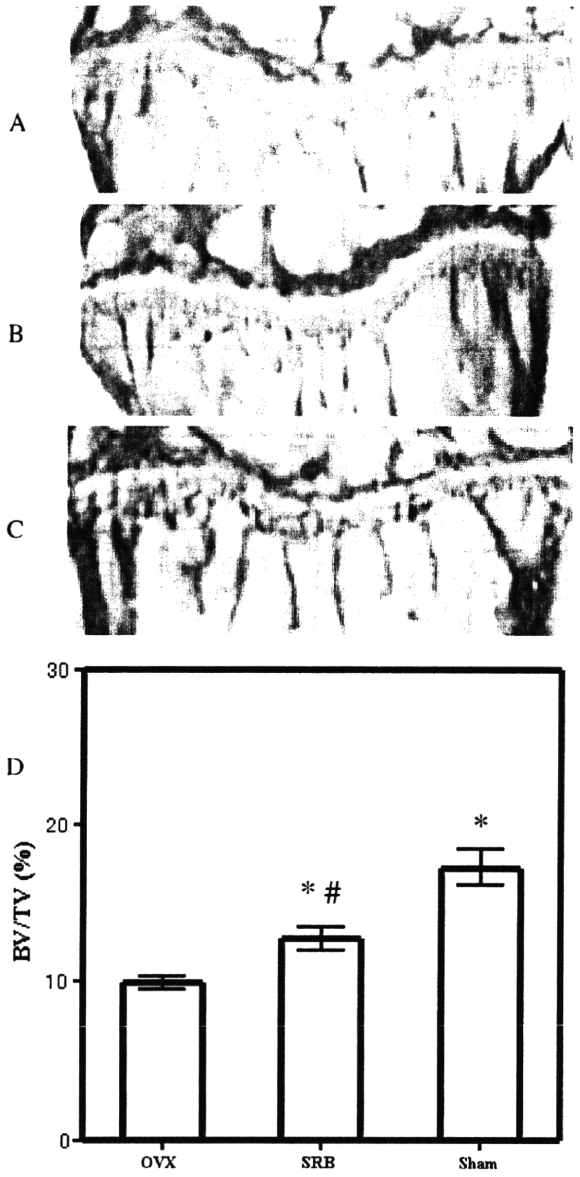

Fig. 3. (A–C) Three-dimensional micro-CT images of proximal tibias from C57BL/6N mice. (A) OVX group, (B) SRB group, and (C) sham group. (D) Bone volume (%) of the proximal metaphyseal region of the tibia, as measured by micro-CT. Data are expressed as mean ± SEM. *; significant difference compared with OVX group, #; significant difference compared with sham group.

SRB downregulated serum IL-6 level in ovariectomized mice

Next, we examined the effect of SRB on serum levels of estradiol, total cholesterol, and IL-6, because these are relevant to bone metabolism and change drastically in the perimenopausal period. Serum estradiol level was significantly higher in the sham group than in either the OVX or SRB groups (OVX: 9.5 ± 0.6 pg/ml; SRB: 8.7 ± 0.6 pg/ml; sham: 33.7 ± 3.9 pg/ml; one-way ANOVA, $p < 0.0001$). However, there was no significant difference in serum estradiol levels between the SRB and OVX groups. Total cholesterol was significantly lower in the sham group than in either the OVX or SRB groups, and, unexpectedly, cholesterol level was not suppressed in the SRB group (OVX: 87.5 ± 5.2 mg/ml; SRB: 85.3 ± 4.3 mg/ml; sham: 70.6 ± 7.4 mg/ml; one-way ANOVA, $p = 0.01$). Serum IL-6 levels were significantly lower in the SRB and sham groups than in the OVX group; IL-6 level did not increase in the SRB group despite ovariectomy (OVX: 138.0 ± 23.1 pg/ml; SRB: 52.5 ± 6.8 pg/ml; sham: 99.7 ± 19.3 pg/ml; one-way ANOVA, $p = 0.02$).

Discussion

Estrogen deficiency in postmenopausal women results in enhanced bone resorption that leads to osteoporosis. For treatment and prevention of osteoporosis, raloxifene and the bisphosphonates are currently the preferred therapy. These agents effectively decrease bone resorption and increase bone mineral density, and reduce the risk of vertebral and other fractures (Delmas et al., 1997; Poole and Compston, 2007); however, they are associated with an increase in the incidence of fatal stroke, venous thromboembolic events (Barrett-Connor et al., 2006), osteonecrosis of the jaw, and gastrointestinal side effects (Ruggiero et al., 2004; Turbi et al., 2004). Hence, further therapeutic options for osteoporosis are needed.

In recent years, various Kampo medicines have been studied for their preventive effects on osteoporosis. Hachimijiogan, Juzentaihoto and Unkeito can improve ovarian function, so these three formulae were indicated to be useful for preventing postmenopausal osteoporosis (Hidaka et al., 1997; Okamoto et al., 1998; Chen et al., 2005). Yao et al. also reported that Goshajinkigan reduced trabecular bone loss as assessed by micro-CT in ovariectomized rats (Yao et al., 2007). Hidaka's group measured bone mineral density (BMD) and performed scanning electron micrography (SEM) in rats with osteoporosis and reported that Chujoto had similar efficacy to 17β-oestradiol in treatment (Hidaka et al., 1999). Dae-bo-won-chun is also reportedly effective in preventing bone loss, and it suppresses the mechanical weakening of the femoral neck in ovariectomized rats (Chae et al., 2001). In addition, several *in vitro* studies have clarified how Kampo medicines work on bone metabolism (Li et al., 1998; Li et al., 1999; Shi et al., 2006). These studies indicate that several Kampo medicines can prevent osteoporosis.

Some studies have shown that lipid-lowering drugs reduce osteoporosis (Edwards et al., 2000; Mundy et al., 1999; Wang et al., 2000). Since SRB was reported to have an effect on hyperlipidemia (Yamada et al., 1998), we herein tested the hypothesis that SRB reduces bone loss in a postmenopausal model.

Using micro-CT, we showed that bone volume of the proximal tibia of SRB-treated mice was significantly greater than that of mice in the OVX group. Bone histomorphometric analysis of lumbar vertebrae also showed that SRB prevented the ovariectomy-induced loss of bone volume. In the SRB group, restoration of bone mass was more prominent for the spine than for the tibia. This finding was supported by previous studies, which revealed that bone loss in OVX rats was more rapid at appendicular bone sites (e.g., the tibia) than at axial bone sites (e.g., the lumbar vertebra) (Cui et al., 2004; Ke et al., 1995). A significant decrease in eroded surface and trends toward decreased osteoblast and osteoclast surfaces were also observed in SRB-treated ovariectomized mice compared with mice that underwent ovariectomy alone. These findings imply that SRB suppressed the rapid increase in bone turnover after ovariectomy. Bone formation indices such as MAR and BFR were not altered by SRB in ovariectomized mice. Taken together, these findings suggest that the protective effects of SRB on bone in ovariectomized mice are likely due to a suppression of bone resorption.

Unkeito, another Kampo medicine, has an estrogen-like effect and prevents the development of bone loss induced by ovariectomy in rats (Chen et al., 2005). However, the present study showed that SRB did not alter serum estradiol in ovariectomized mice. Although

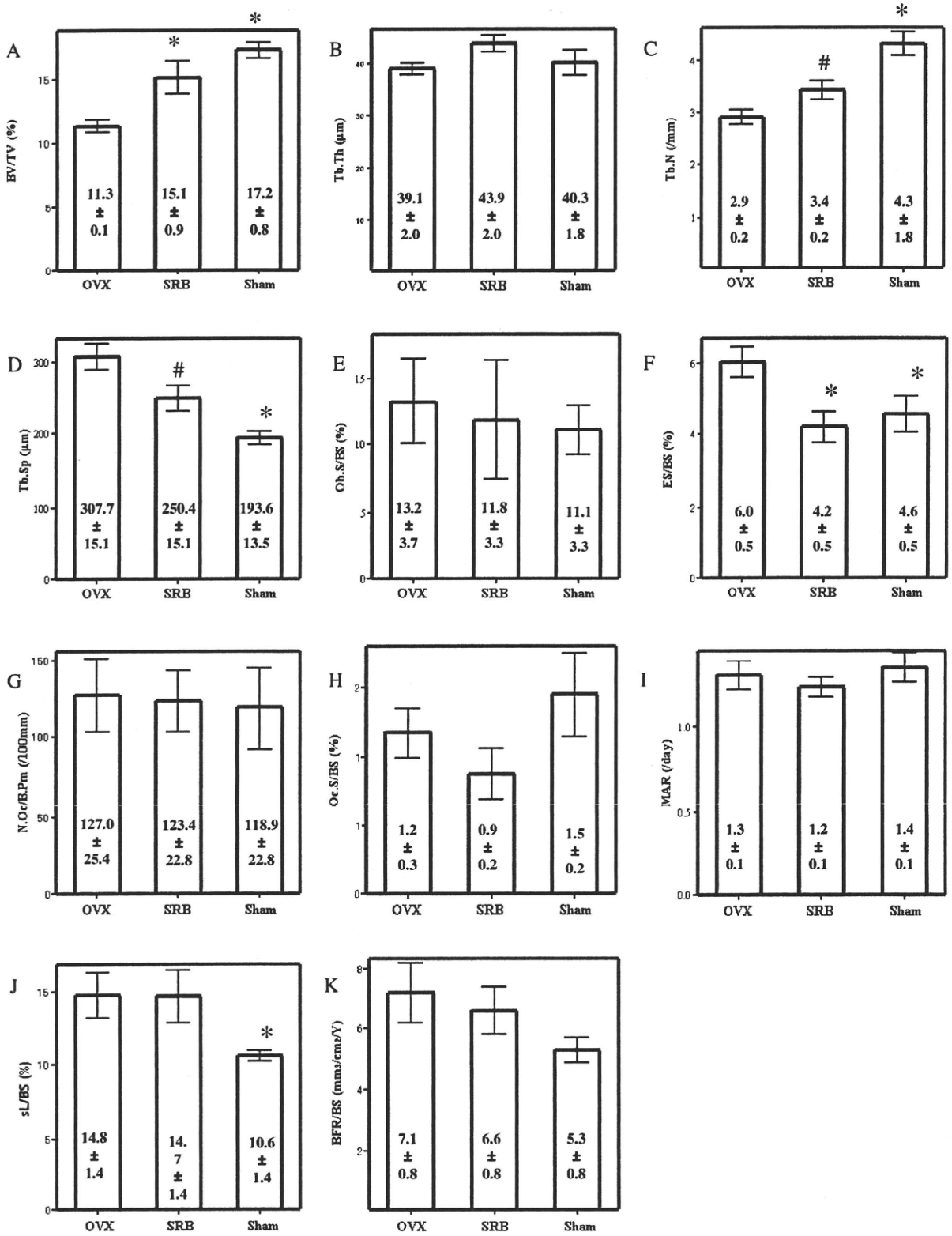

Fig. 4. Histomorphometric analysis of trabecular bone in the lumbar spine. (A) bone volume/tissue volume (BV/TV); (B) trabecular thickness (Tb.Th); (C) trabecular number (Tb.N); (D) trabecular space (Tb.Sp); (E) osteoblast surface/bone surface (Ob.S/BS); (F) eroded surface/bone surface (ES/BS); (G) osteoblast number/bone perimeter (N.Oc/BPm); (H) osteoclast surface/bone surface (Oc.S/BS); (I) mineral apposition rate (MAR); (J) mineralizing surface; single labeled surface/bone surface (sL/BS); (K) bone formation rate/bone surface (BFR/BS). Data are expressed as mean ± SEM. *; significant difference when compared with OVX group, #; significant difference when compared with sham group.

SRB and the extracts of *Zingiber officinale* and *Cinnamomum cassia* have previously been reported to have beneficial effects against hyperlipidemia, SRB did not affect serum total cholesterol level in the present study. This indicates that SRB could decrease serum total cholesterol level in a hyperlipidemia model (Chung et al., 2003; Yoshie et al., 2001) or *in vitro* (Kannappan et al., 2006; Matsuda et al., 2009), but not in an ovariectomy model.

Several reports show that IL-6 and other cytokines mediate bone loss induced by estrogen deficiency (Jika et al., 1992; Poli et al., 1994). In the presence of estrogen, IL-6 expression is suppressed, but its level increases in the absence of estrogen, and several clinical studies have shown high serum IL-6 levels among postmenopausal women (Pacifici et al., 1991). IL-6 is suggested to be a primary mediator of bone resorption through induction of osteoclastogenesis (Flanagan et al., 1995). IL-6 upregulation has an important role in the development of osteoporosis in ovariectomized mice and can be inhibited by androgen or IL-6 neutralizing antibody (Bellido et al., 1995). The present study showed that serum IL-6 levels in the SRB group were significantly lower than in the OVX group, suggesting that SRB can decrease serum IL-6 levels in this postmenopausal model.

Our histomorphometric results showed that the eroded surface (an indicator of osteoclast activity) was significantly smaller in the SRB group than in the OVX group. This lends support to the premise that SRB suppressed osteoclastogenesis by reducing serum IL-6 level. In our study, ovariectomized mice were not administered other therapies such as replacement estrogen therapy, which would have increased bone density and decreased serum IL-6. In that sense, we did not use any positive controls in this experiment. However, the comparison of bone and serum data with the OVX group support the idea that administration of SRB in a postmenopausal-osteoporosis model had an effect on preventing loss of bone volume and suppressing serum IL-6 levels.

Expression of IL-6 is largely controlled by nuclear factor-κB (NFκB) (Libermann and Baltimore, 1990). NFκB is an inducible dimeric transcription factor that belongs to the Rel/NFκB family of transcription factors. In resting cells, NFκB is sequestered in the cytoplasm by IκB proteins. Stimulus-mediated phosphorylation and subsequent proteolytic degradation of IκB allows the release and nuclear translocation of NFκB, where it transactivates a number of target genes. Recently, it was reported that saikosaponin, a principal component of SRB, inhibited T cell activation via the suppression of NFκB (Leung et al., 2005). Dang et al. (2007) reported that saikosaponin attenuated CCl_4-induced hepatic fibrosis via downregulation of TNFα, IL-6, and NFκB expression. Thus, one of the mechanisms by which SRB prevents the development of bone loss might be suppression of the expression of IL-6 via NFκB inactivation. Extracts of *Cinnamomum cassia*, *Zingiber officinale* and *Panax ginseng*, which represent the principal components of SRB, reportedly suppress osteoclastogenesis (Han et al., 2007; Liu et al., 2009; Sung et al., 2009; Tsuji-Naito, 2008). Incorporating these herbal medicines would thus also contribute to the prevention of bone loss.

Conclusions

We showed that SRB can prevent loss of bone volume and suppress serum IL-6 level in a postmenopausal model. Our results suggest that SRB deserves further investigation as a therapeutic option for treatment of postmenopausal osteoporosis.

Acknowledgments

We would like to thank Drs. Masafumi Kashii and Junko Murai for their helpful advice on the OVX experiment, and Yasuo Tsukamoto, Yousuke Hashimoto, Akitoshi Asami and Naoko Hattori for their excellent pharmacological advice.

References

Barrett-Connor, E., Mosca, L., Collins, P., Geiger, M.J., Grady, D., Kornitzer, M., McNabb, M.A., Wenger, N.K., Raloxifene Use for The Heart (RUTH) Trial Investigators, 2006. Effects of raloxifene on cardiovascular events and breast cancer in postmenopausal women. The New England Journal of Medicine 13,355 (2), 125–137.

Bellido, T., Jilka, R.L., Boyce, B.F., Girasole, G., Broxmeyer, H., Dalrymple, S.A., Murray, R., Manolagas, S.C., 1995. Regulation of interleukin-6, osteoclastogenesis, and bone mass by androgens: the role of the androgen receptor. The Journal of Clinical Investigation 95 (6), 2886–2895.

Chae, H.J., Kang, J.S., Kim, J.H., Kim, C.W., Yoo, S.K., Shin, T.Y., Choi, B., Kim, H.M., Kim, H.R., 2001. Antiosteoporotic activity of Dae-Bo-Won-Chun in ovariectomized rats. Phytotherapy Research 15 (1), 53–57.

Chen, H., Emura, S., Isono, H., Shoumura, S., 2005. Effects of traditional Chinese medicine on bone loss in SAMP6: a murine model for senile osteoporosis. Biological & Pharmaceutical Bulletin 28 (5), 865–869.

Chung, H.J., Maruyama, I., Tani, T., 2003. Saiko-ka-ryu-kotsu-borei-to inhibits intimal thickening in carotid artery after balloon endothelial denudation in cholesterol-fed rats. Boilogical & Pharmaceutical Bulletin 26 (1), 56–60.

Cui, L., Wu, T., Deng, Y.Y., Ai, C.M., Chen, H.Q., 2004. Tanshinone prevents cancellous bone loss induced by ovariectomy in rats. Acta Pharmacologica Sinica 25 (5), 678–684.

Dang, S.S., Wang, B.F., Cheng, Y.A., Song, P., Liu, Z.G., Li, Z.F., 2007. Inhibitory effects of saikosaponin-d on CCl4-induced hepatic fibrogenesis in rats. World Journal of Gastroenterology 13 (4), 557–563.

Delmas, P.D., Bjarnason, N.H., Mitlak, B.H., Ravoux, A.C., Shah, A.S., Huster, W.J., Draper, M., Christiansen, C., 1997. Effects of raloxifene on bone mineral density, serum cholesterol concentrations, and uterine endometrium in pistmenopausal women. The New England Journal of Medicine 4, 1641–1647.

Edwards, C.J., Hart, D.J., Spector, T.D., 2000. Oral statins and increased bone-mineral density in postmenopausal women. Lancet 355 (9222), 2218–2219.

Flanagan, A.M., Stow, M.D., Williams, R., 1995. The effect of inteleukin-6 and soluble interleukin-6 receptor protein on the bone resorptive activity of human osteoclasts generated in vitro. The Journal of Pathology 176 (3), 289–297.

Han, S.Y., Lee, J.R., Kwon, Y.K., Jo, M.J., Park, S.J., Kim, S.C., Lee, H.S., Ku, S.K., 2007. Ostreae Testa prevent ovariectomy-induced bone loss in mice by osteoblast activations. Journal of Ethnopharmacology 114 (3), 400–405.

Hill, K., 1996. The demography of menopause. Maturitas 23 (2), 113–127.

Hidaka, S., Okamoto, Y., Nakajima, K., Suekawa, M., Liu, S.Y., 1997. Preventive effects of traditional Chinese (Kampo) medicines on experimental osteoporosis induced by ovariectomy in rats. Calcified Tissue International 61 (3), 239–246.

Hidaka, S., Okamoto, Y., Yamada, Y., Kon, Y., Kimura, T., 1999. A Japanese herbal medicine, Chujo-to, has a benefical effect on osteoporosis in rats. Phytotherapy Research 13 (1), 14–19.

Hodsman, A.B., 2001. Fragility fractures in dialysis and transplant patients. Is it osteoporosis, and how should it be treated? Peritoneal Dialysis International 21 (Suppl. 3), S247–S255.

Jika, R.L., Hangoc, G., Girasole, G., Passeri, G., Williams, D.C., Abrams, J.S., Boyce, B., Broxmeyer, H., Manolagas, S.C., 1992. Increased osteoclast debelopment after estrogen loss: mediation by interleukin-6. Science 257 (5066), 88–91.

Kannappan, S., Jayaraman, T., Rajasekar, P., Ravichandran, M.K., Anuradha, C.V., 2006. Cinnamon bark extract improves glucose metabolism and lipid profile in the fructose-fed rat. Singapore Medical Journal 47 (10), 858–863.

Ke, H.Z., Chen, H.K., Qi, H., Pirie, C.M., Simmons, H.A., Ma, Y.F., Thompson, D.D., 1995. Effects of droloxifene on prevention of cancellous bone loss and bone turnover in the axial skeleton of aged, ovariectomized rats. Bone 17, 491–496.

Leung, C.Y., Liu, L., Wong, R.N., Zeng, Y.Y., Li, M., Zhou, H., 2005. Saikosaponin-d inhibits T cell activation through the modulation of PKCtheta, JNK, and NF-kappaB transcription factor. Biochemical and Biophysical Research Communications 338 (4), 1920–1927.

Li, H., Miyahara, T., Tezuka, Y., Namba, T., Nemoto, N., Tonami, S., Seto, H., Tada, T., Kadota, S., 1998. The effect of Kampo formulae on bone resorption in vitro and in vivo.1. Active constituents of Tsu-kan-gan. Biological Pharmaceutical Bulletin 21 (12), 1322–1326.

Li, H., Miyahara, T., Tezuka, Y., Namba, T., Suzuki, T., Dowaki, R., Watanabe, M., Nemoto, N., Tonami, S., Seto, H., Kadota, S., 1999. The effect of Kampo formulae on bone resorption in vitro and in vivo. 2. Detailed study of berberine. Biological & Pharmaceutical Bulletin 22 (4), 391–396.

Libermann, T.A., Baltimore, D., 1990. Activation of interleukin-6 gene expression through the NF-kappa B transcription Factor. Molecular and Cellular Biology 10 (5), 2327–2334.

Liu, J., Shiono, J., Shimizu, K., Yu, H., Zhang, C., Jin, F., Kondo, R., 2009. 20(R)-ginsenoside Rh2, not 20(S), is a selective osteoclastgenesis inhibitor without

any cytotoxicity. Bioorganic & Medical Chemistry Letters 19 (12), 3320–3323.
Matsuda, A., Wang, Z., Takahashi, S., Tokuda, T., Miura, N., Hasegawa, J., 2009. Upregulation of mRNA of retinoid binding protein and fatty acid binding protein by cholesterol enriched-diet and effect of ginger on lipid metabolism. Life Science 84 (25–26), 903–907.
Melton III, L.J., Kan, S.H., Frye, M.A., Wahner, H.W., O'Fallon, W.M., Riggs, B.L., 1989. Epidemiology of vertebral fractures in woman. American Journal of Epidemiology 129 (5), 1000–1011.
Mundy, G., Garrett, R., Harris, S., Chan, J., Chen, D., Rossini, G., Boyce, B., Zhao, M., Gutierrez, G., 1999. Stimulation of bone formation in vitro and in rodents by statins. Science 286 (5446), 1946–1949.
Okamoto, Y., Hidaka, S., Yamada, Y., Ouchi, K., Miyazaki, K., Liu, S.Y., 1998. Thermal analysis of bones from ovariectomized rats. Journal of Biomedical Materials Research 41 (2), 221–226.
Pacifici, R., Brown, C., Puscheck, E., Friedrich, E., Slatopolsky, E., Maggio, D., McCracken, R., Avioli, L.V., 1991. Effect of surgical menopause and estrogen replacement on cytokine release from human blood mononuclear cells. Proceedings of the National Academy of Sciences of the Unites States of America 88 (12), 5134–5138.
Perfitt, A.M., Drezner, M.K., Glorieux, F.H., Kanis, J.A., Malluche, H., Meunier, P.J., Ott, S.M., Recker, R.R., 1987. Bone histomorphometry: standardization of nomenclature, symbols, and units. Report of the ASBMR Histrmorphometry Nomenclature Committee. Journal of Bone and Mineral Reseach 2 (6), 595–610.
Poli, V., Balena, R., Fattori, E., Markatos, A., Yamamoto, M., Tanaka, H., Ciliberto, G., Rodan, G.A., Costantini, F., 1994. Interleukin-6 deficient mice are protected from bone loss caused by estrogen depletion. The EMBO Journal 13 (5), 1189–1196.
Poole, K.E., Compston, J.E., 2007. Osteoporosis and its management. BMJ 16, 1251–1256.
Ray, W.A., Daugherty, J.R., Griffin, M.R., 2002. Lipid-lowering agents and the risk of hip fracture in a Medicaid population. Injury Prevention 8 (4), 276–279.
Riggs, B.L., Melton 3rd, L.J., 1995. The worldwide problem of osteoporosis: insights afforded by epidemiology. Bone 17 (5), 505S–511S.
Ruggiero, S.L., Mehrotra, B., Rosenberg, T.J., Engroff, S.L., 2004. Osteonecrosis of the jaws associated with the use of bisphosphonates: a review if 63 cases. Journal of Oral and Maxillofacial Surgery 62 (5), 527–534.
Shi, L., Tezuka, Y., Subehan, Ueda, J., Miyahara, T., Yin, J., Nobukawa, T., Kadota, S., 2006. Inhibitory effect of kampo medicines on bone resorption in vitro and preventive effect on bone loss in vivo. Journal of Traditional Medicines 23, 92–100.
Sung, B., Murakami, A., Oyajobi, B.O., Aggarwal, B.B., 2009. Zerumbone abolishes RANKL-induced NF-kappaB activation, inhibits osteoclastogenesis, and suppresses human breast cancer-induced bone loss inathymic nude mice. Cancer Research 69 (4), 1477–1484.
Tsuji-Naito, K., 2008. Aldehydic components of cinnamon bark extract suppresses RANKL-induced osteoclastogenesis through NFATc1 downregulation. Bioorganic & Medical Journal 16 (20), 9176–9183.
Turbi, C., Herrero-Beaumont, G., Acebes, J.C., Torrijos, A., Grana, J., Miquelez, R., Sacristan, J., Marin, F., 2004. Compliance and satisfaction with raloxifene versus alendronate for the treatment of postmenopausal osteoporosis in clinical practice: an open-label, prospective, nonrandomized, observational study. Clincal Therapeutics 26 (2), 245–256.
Wang, P.S., Solomon, D.H., Mogun, H., Avorn, J., 2000. HMG-CoA reductase inhibitors and the risk of hip fractures in elderly patients. JAMA 283 (24), 3211–3216.
Yamada, T., Satoh, S., Katoh, S., Mizuno, G., Yoshomura, M., Sakurai, I., 1998. Pathological analysis on the effects of traditional Chinese drugs in spontaneously hypertensive rats (SHR) aorta. Doumyakukouka 16, 999–1007.
Yao, X., Chen, H., Emura, S., Otake, N., Shoumura, S., 2007. Effects of hPTH (1-34) and Gosha-jinki-gan on the trabecular bone microarchitecture in ovariectomized rat tibia. Okajimas Folia Anatomica Japonica 83 (4), 107–113.
Yoshie, F., Iizuka, A., Kubo, M., Komatsu, Y., Matsumoto, A., Itakura, H., Takeda., H., Matsumiya, T., Kondo, K., 2001. Protective effects of saiko-ka-ryu-kotsu-borei-to (Chai-Hu-Jia-Long-Gu-Mu-Li-Tang) against atherisclerosis in Kurosawa and Kusanagi-hypercholesterolemic (KHC) rabbits. Pharmacogical Research 43 (5), 481–488.

Clinical & Experimental Immunology
The Journal of Translational Immunology

Clinical and Experimental Immunology ORIGINAL ARTICLE doi:10.1111/j.1365-2249.2010.04163.x

TP53 mutations coincide with the ectopic expression of activation-induced cytidine deaminase in the fibroblast-like synoviocytes derived from a fraction of patients with rheumatoid arthritis

H. Igarashi,* J. Hashimoto,† T. Tomita,† H. Yoshikawa† and K. Ishihara*

**Department of Immunology and Molecular Genetics, Kawasaki Medical School, Kurashiki City, Okayama, and †Department of Orthopaedics, Osaka University Graduate School of Medicine, Suita City, Osaka, Japan*

Accepted for publication 24 February 2010
Correspondence: K. Ishihara, Department of Immunology and Molecular Genetics, Kawasaki Medical School, 577 Matsushima, Kurashiki City, Okayama 701-0192, Japan.
E-mail: ishihara-im@med.kawasaki-m.ac.jp

Summary

Main features of rheumatoid arthritis (RA), hyperplasia of fibroblast-like synoviocytes (FLS) and joint destruction are caused by inflammatory cytokines produced in chronic autoimmune inflammation. Cell-intrinsic acquisition of tumour-like phenotypes of RA-FLS could also be responsible for the aggressive proliferation and invasion, which are supported by the fact that in some cases RA-FLS has mutations of a tumour suppressor gene *TP53*. However, the underlying molecular mechanism for *TP53* mutations in RA-FLS has not yet been clarified. Recently it has been reported that the non-lymphoid cells in the inflammatory tissues express ectopically the *activation-induced cytidine deaminase (AID)* gene that induces somatic hypermutations, not only at the immunoglobulin (Ig) gene variable regions in germinal centre B lymphocytes but also at coding regions in *TP53*. Real-time polymerase chain reaction (PCR) analyses revealed more than half (five of nine) of the RA-FLS lines we established showed the markedly increased expression of *AID*. *AID* transcription in RA-FLS was augmented by tumour necrosis factor (TNF)-α and even by physiological concentration of β-oestradiol that could not induce *AID* transcription in osteoarthritis-FLS. Furthermore, AID-positive RA-FLS presented a higher frequency of somatic mutations in *TP53*. Cytological and immunohistochemical analyses demonstrated clearly the ectopic expression of *AID* in the FLS at the RA synovium. These data suggested strongly a novel consequence of RA; the ectopic expression of AID in RA-FLS causes the somatic mutations and dysfunction of *TP53*, leading to acquisition of tumour-like properties by RA-FLS.

Keywords: human, rheumatoid arthritis, somatic mutation, synoviocyte

Introduction

Rheumatoid arthritis (RA) is a systemic autoimmune disease in which the joints are chronically inflamed and the cartilage and bone are destroyed by pannus formation, which is the invasion of cartilage and bone by proliferating fibroblast-like synoviocytes (FLS) [1–3]. The incidence of RA is correlated with certain human leucocyte antigen D-related (HLA-DR) haplotypes and the presence of autoantibodies, such as rheumatoid factor (RF) and anti-cyclic citrullinated peptide (CCP) antibody, suggesting strongly the involvement of the deregulated immune system; T helper type 17 (Th17), a novel helper T cell subset producing interleukin (IL)-17, has become a topic as a player in local inflammation driven by acquired immunity [4,5]. However, details of the pathophysiology of RA is not understood completely [6]. Local cytokines such as basic fibroblast growth factor (bFGF), platelet-derived growth factor (PDGF), transforming growth factor (TGF)-β, tumour necrosis factor (TNF)-α and IL-1β are considered to be responsible for the hyperplasia of FLS [7,8]. Upon activation, FLS produce TNF-α, IL-1β, IL-6 and matrix metalloproteinases, establishing the chronic and destructive inflammatory circuit [2]. The critical roles of these inflammatory cytokines have been shown by the effectiveness of cytokine-blockade therapies using anti-TNF-α or anti-IL-6 receptor antibodies for the treatment of RA [9,10]. However, it has also been recognized that certain RA subsets are resistant to these anti-cytokine therapies [11]. Such resistance may be explained partly by the intrinsic abnormality of RA-FLS independent of inflammation. Accumulated evidence has indicated that RA-FLS are stably activated and exhibit tumour-like characteristics. For example, they

destroyed human cartilage when they were transplanted together into severe combined immunodeficiency (SCID) mice [12]. RA-FLS expressed high levels of proto-oncogenes such as *c-myc* and *c-fos* [13,14]. In addition to these findings, RA-FLS are reported to express the tumour suppressor gene *TP53* with somatic mutations [15–19], and down-regulate the tumour suppressor *PTEN*, a protein phosphatase gene [20]. In particular, the somatic mutation of the *TP53* gene in RA-FLS appears consistent not only with their increased resistance to apoptosis but also with their proinflammatory properties such as the production of IL-6 and matrix metalloproteinase (MMP)-1 [21–23]. However, little is known about the mechanism by which the somatic mutations are introduced into the *TP53* gene in RA-FLS.

Activation-induced cytidine deaminase (AID) is a member of the APOBEC family, which is a cellular cytidine deaminase involved in protection from retrovirus infection or regulation of cholesterol metabolism [24]. AID was identified originally as an indispensable molecule for somatic hypermutation (SHM) at the immunoglobulin variable region and class-switch recombination in germinal centre B lymphocytes [25,26]. Recently, several papers have demonstrated that *AID* was up-regulated in non-lymphoid tumour cells such as breast cancer, cholangiocarcinoma, hepatoma and colorectal cancer cells [27–33]. Moreover, the somatic mutations of *TP53* found in these cancer cells appeared to be a direct target of AID [29,30].

In our study, we demonstrated that AID was expressed selectively by a fraction of RA-FLS, and that it was associated with somatic mutations in *TP53*. This suggests a possible mechanism by which the aberrant expression of AID within certain RA-FLS induces somatic mutations in *TP53*, leading to the acquisition of proinflammatory or tumour-like phenotypes.

Materials and methods

Cells and cell culture

Transformed human FLS cell lines were established from the synovial tissues of RA ($n = 9$; five males and four females) and osteoarthritis (OA) ($n = 9$; nine females) patients at the time of joint replacement surgery (Table 1). The tissues were obtained with the informed consent of the patients. Briefly, the synovial tissues were minced into small pieces and dissociated with collagenase and hyarulonidase in DMEM at 37°C for 1 h with shaking. After passing through mesh and washing with Dulbecco's modified Eagle's medium (DMEM), the synovial cells were suspended in the culture medium [DMEM containing 10% fetal calf serum (FCS) and penicillin/streptomycin] and plated in dishes. On the next day, non-adherent cells were removed and the medium was refreshed. The synovial cells were cultured in 10% CO_2 at 37°C with humidified air. After four passages, when it was ensured that no haematopoietic cells were present in the cell lines, plasmids pAct-SVT containing SV40T antigen were transduced with lipofectamine 2000 (Invitrogen, Carlsbad, CA, USA). All the cell lines showed fibroblast-like morphology and expressed CD44, CD106 and CD157/BST-1 on their surfaces, characteristic of synovial fibroblasts (data not shown). The transformed and original non-transformed primary FLS cells were maintained in DMEM supplemented with 10% heat-inactivated FCS with antibiotics. Materials for mRNA and protein analyses were obtained from the cell lines with passage numbers of <8 after thawing the frozen stocks. This study protocol was approved by the institutional review boards for ethics at the Faculty of Medicine, Osaka University (no. 340-1) and the Kawasaki Medical School (no. 291). For cell stimulation, FLS were cultured in phenol red-free DMEM (Sigma-Aldrich, St Louis, MO, USA) complete medium in the presence or absence of TNF-α (50 ng/ml; Pepro Tech Inc., Rocky Hill, NJ, USA), β-oestradiol (E_2; 10^{-9} M; Sigma-Aldrich) or both for 24 h.

Table 1. Characteristics of the patients in the study of transformed fibroblast-like synoviocytes.

	OA ($n = 9$)	RA ($n = 9$)
Age, mean (range) years	70·7 (64–80)	61·3 (35–75)
Sex, no. female/male	9/0	4/5
Disease duration, mean (range) years	n.a.	9·9 (4–19)
Medications, no. taking/no. assessed		
NSAIDs	9/9	6/9
DMARDs	0/9	7/9
Plus steroids	0/9	5/9
Soluble TNFR	0/9	1/9
No. RF+(>20IU)/no. assessed	n.a.	7/8
CRP, mean (range) mg/dl	n.a.	2·8 (0·7–5·3)
MMP-3, mean (range) ng/ml	n.a.	424·1 (49·7–973)

CRP, C-reactive protein; DMARDs, disease-modifying anti-rheumatic drugs; MMP, matrix metalloproteinase; n.a., not assessed; NSAID, non-steroidal anti-inflammatory drugs; OA, osteoarthritis; RF, rheumatoid factor; TNF, tumour necrosis factor.

Non-quantitative reverse transcription–polymerase chain reaction (RT–PCR) and quantitative real-time RT–PCR

Total RNAs were extracted using TRIzol® (Invitrogen), according to the manufacturer's instructions. Random hexamer-primed cDNAs were prepared using the ReverTra Ace® RT kit (Toyobo, Osaka, Japan) with 1 μg of total RNA and amplified by PCR using KOD-FX (Toyobo). The synthetic oligonucleotide primers for amplification of *AID*, *APOBEC1* and *APOBEC3G* were as follows: *AID*, 5′-AAATGTCCGCTGGGCTAAGG-3′ (forward) and 5′-GG AGGAAGAGCAATTCCACGT-3′ (reverse) [28]; *APOBEC1*, 5′-GGGACCTTGTTAACAGTGGAGT-3′ (forward) and 5′-CCAGGTGGGTAGTTGACAAAA-3′ (reverse); *APOBEC3G*,

5′-GAGCGCATGCACAATGAC-3′ (forward) and 5′-GCC TTCAAGGAAACCGTGT-3′ (reverse). The latter two primer sets were synthesized using Primer-BLAST (NCBI). The PCR for CD19 to exclude the contamination of B cells in FLS lines was conducted with the following primers: 5′-GACCTC ACCATGGCCCCTGG-3′ (forward) and 5′-CAGCCAG TGCCATAGTAC-3′ (reverse) [34]. The specific primers for human *AID* for quantitative real-time RT–PCR were designed using the Universal Primer Design Tools available on the Roche website. The 6-carboxyfluorescein-labelled probe for human *AID* was obtained from Roche (Universal Probe Library, probe no. 69; Roche Diagnostics, Indianapolis, IN, USA). The expression levels of target cDNAs were normalized to the endogenous transcription levels of human *GAPDH*. Gene expression was quantified using the 7500 real-time PCR system (PE Applied Biosystems, Foster City, CA, USA).

Western blot analysis

Whole-cell lysates (equivalent to 25 μg) in 1% TNE lysis buffer [1% Nonidet-P40, 150 mM NaCl, 10 mM Tris-HCl, pH 7·5, 1 mM ethylenediamine tetraacetic acid (EDTA)], in the presence of a protease inhibitor cocktail (Sigma-Aldrich) and protein kinase/phosphatase inhibitor cocktail (Roche) were subjected to Western blot analysis using polyvinylidine fluoride membrane and signal-enhancing kit (Santa Cruz Biotechnology Inc., Santa Cruz, CA, USA). The membrane was probed with rabbit anti-human AID antibody (Abcam, Cambridge, MA, USA) and reprobed with anti-β-actin antibody (Santa Cruz).

Immunocytochemistry and immunohistochemistry

We cultured 2×10^4 cells on the culture slide chamber (BD Falcon, Franklin Lakes, NJ, USA) for 12 h. After fixation with chilled acetone, the cells were washed and then blocked with 3% bovine serum albumin (BSA) in PBS. The cells were immunostained with either rabbit anti-human AID antibody (Abcam) combined with horseradish peroxidase-conjugated goat anti-rabbit immunoglobulin (Ig)G antibody (Southern Biotech, Birmingham, AL, USA) or with rat anti-human AID monoclonal antibody (mAb) (EK2 5G9; Cell Signaling Tech. Inc., Danvers, MA, USA) combined with biotinylated donkey anti-rat IgG antibody (Jackson ImmunoResearch Laboratories, Inc., West Grove, PA, USA) and vectastain elite ABC kit (Vector Laboratories Inc., Burlingame, CA, USA). The bound antibodies were visualized using diaminobenzidine (DAB) and counterstaining with haematoxylin. The images were obtained using a bright-field microscope (Axiophot, Carl Zeiss, Munich, Germany).

Cryosections with 6 μm thickness of the synovial tissues from RA patients were also stained with rat anti-human AID mAb after fixation with chilled acetone and detected as described above. The endogenous peroxidase activity was inactivated by treatment with 0·01% H_2O_2/PBS for 10 min at room temperature. Non-specific binding of second antibodies was blocked with PBS containing 5% of either normal goat or donkey serum for 30 min. To identify B cell follicles, mouse anti-human CD20 (Dako, Glostrup, Denmark) mAb and Envision goat anti-mouse and rabbit IgG antibody conjugated with horseradish peroxidase (Dako) were used. Rat anti-mouse CD4 mAb (GK1·5) was used as an isotype-matched control. For immunofluorescence staining, cryosections with 6 μm thickness of the synovial tissues from RA patients were fixed and stained with rat anti-human AID mAb and mouse anti-human CD20, the same as above. Either donkey anti-rat IgG antibody conjugated with Alexa 488 or donkey anti-mouse IgG antibody conjugated with Alexa 594 were used as second antibodies. Fluorescence images were obtained under the fluorescence microscope (Eclipse E800, Nikon, Tokyo, Japan).

Mutation analysis of TP53

The coding region of *TP53* spanning from exons 4–11 was amplified using high-fidelity DNA polymerase (iProof™, Bio-Rad, Hercules, CA, USA) with forward and reverse primers containing the *Sal*I and *Eco*RI sequences, respectively, as follows: forward, 5′-GCGTCGACCTACCAGGGC AGCTACGGTTTC-3′ and reverse, 5′-GGAATTCTTATGGC GGGAGGTAGACTGACC-3′. The amplicon was digested using restriction enzymes and subcloned into the corresponding cloning sites of the pBluescript vector. The insertion was sequenced with both the T3 and T7 primers located upstream and downstream of the cloning site, respectively, in pBluescript using sequence detector (Applied Biosystems). From the amplicons prepared from one FLS line, more than 35 colonies were picked up after bacterial transformation and each PCR product were sequenced. The sequence data were compared with those of the *TP53* nucleotide sequence obtained from GenBank (Accession number: NM_000546).

Results

Aberrant expression of AID in RA-FLS

First, we assessed the expression of the *AID* gene in transformed FLS cell lines obtained from OA and RA patients by RT–PCR. Surprisingly, *AID* was transcribed in more than half the RA-FLS lines (five of nine) and in none of the OA-FLS lines (Fig. 1a). In the RA-FLS lines *APOBEC1* was not expressed, whereas *APOBEC3G* was expressed ubiquitously, suggesting that *AID* transcription in RA-FLS is selective (Fig. 1a). Then, we used real-time PCR to quantify *AID* transcription among FLS. The same sets of RA-FLS showed approximately 7–18-fold higher *AID* transcription compared to the FLS from OA2 (Fig. 1b) that expressed a low but detectable level of AID transcription. Due probably to the higher sensitivity of probe-based real-time PCR, negligible

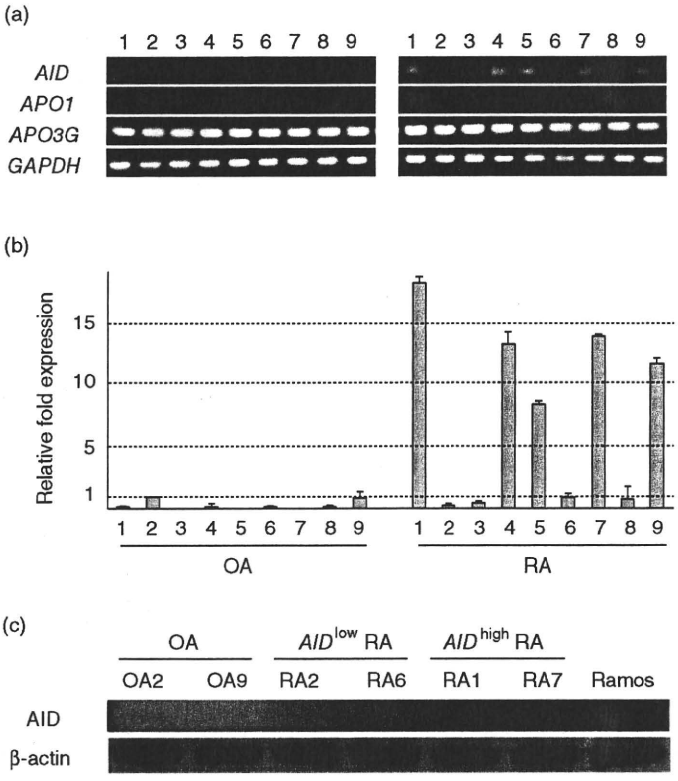

Fig. 1. Endogenous expression of activation-induced cytidine deaminase (AID) in rheumatoid arthritis-fibroblast-like synoviocytes (RA-FLS) lines. (a) The ectopic transcription of *AID* was detected in RA-FLS lines by reverse transcription–polymerase chain reaction (RT–PCR). The expression of two other APOBEC family members (*APO1*: APOBEC1, *APO3G*: APOBEC3G) was also examined by RT–PCR. (b) *AID* mRNA was quantified (relative quantification) by real-time PCR and normalized to housekeeping gene, *GAPDH* and fold expression over that of OA-FLS (OA2) was calculated by ΔΔCT method in triplicate. The grey bars and error bars indicate the averages and standard deviations, respectively, of two independent experiments. (c) Crude protein extracts from the representative FLS lines were analysed by sodium dodecyl sulphate-polyacrylamide gel electrophoresis (SDS-PAGE)/immunoblotting using anti-human AID polyclonal antibody (upper panel) or anti-β-actin (lower panel).

to very low levels of *AID* transcription were detectable by real-time PCR in the other four RA-FLS, as well as in some OA-FLS. Here, five RA-FLS with the expression levels of *AID* higher than fivefold compared with the level of OA2 are defined as AID^{high} FLS (RA1, 4, 5, 7, 9) and the other four RA-FLS (RA2, 3, 6, 8) with the equivalent levels to OA-FLS are defined as AID^{low} FLS. This aberrant expression of *AID* is not likely to have resulted by contamination of B cells expressing *AID*, because the synovial cell culture was occupied with adherent and morphologically fibroblast-like cells after four passages. The possibility of B cell contamination was clearly excluded because no transcription of CD19, a pan B cell marker, was detectable in the AID^{high} FLS (data not shown, but the primer pairs are described in Materials and methods). Next, we confirmed the endogenous expression of the AID protein by Western blot analysis with the two representative cell lines from OA, AID^{low} RA and AID^{high} RA (Fig. 1c).

The aberrant expression of AID in a fraction of RA-FLS prompted us to investigate its correlation with the clinical characteristics in nine RA patients from whom FLS were established. The frequencies of AID^{high} RA-FLS were 75% (three of four) and 40% (two of five) in RA-FLS derived from female and male RA patients, respectively. No correlation was observed in the ages, serum MMP-3 levels or medicines prescribed to the patients. Laboratory data revealed the tendency of higher C-reactive protein (CRP) levels in the AID^{high} RA-FLS than in the AID^{low} RA-FLS (3·9 ± 1·7 *versus* 1·5 ± 0·6, respectively), although the sample size of our study is too small to detect these correlations adequately. These data suggested that AID expression in FLS might be facilitated under conditions of inflammation in female patients. Because inflammatory cytokines and oestrogen have been reported to induce *AID* transcription [28,30,35], we investigated whether this is also the case in FLS. In OA-FLS with low levels of *AID* expression, TNF-α but not physiological concentration of β-oestradiol (E_2) augmented the transcription of *AID*, and simultaneous stimulation with E_2 and TNF-α exhibited synergistic effects (Fig. 2). In AID^{low} RA-FLS, E2 or TNF-α alone enhanced the transcription of *AID* much higher than OA-FLS, although the synergistic effect was not obvious. Even in AID^{high} RA-FLS, E_2 or TNF-α alone augmented the transcription of *AID*, which resulted in more than 20-fold higher levels of *AID* transcription compared with basal levels those in OA-FLS. It is of note that physiological concentration of β-oestradiol up-regulated *AID* transcription only in RA-FLS, suggesting intrinsic RA-FLS abnormality in the susceptibility of *AID* induction to female sex steroids. As another molecular mechanism for *AID* induction, negative regulatory roles for the microRNA miR-155 on AID transcription have been reported in previous studies on germinal centre B cells [36,37], but there was no significant down-regulation of miR-155 in AID^{high} RA-FLS (data not shown). Real-time PCR analyses of RA-FLS did not show *TNF-α* transcription or correlation between the transcription levels of *IL-6* or *IL-1β*